

1 Evaluating a fire smoke simulation
2 algorithm in the National Air Quality
3 Forecast Capability (NAQFC) by using
4 multiple observation data sets during the
5 Southeast Nexus (SENEX) field campaign

6 Li Pan ^{1,2}, HyunCheol Kim ^{3,4}, Pius Lee ³, Rick Saylor ⁵, YouHua Tang ^{3,4}, Daniel Tong ^{3,6}, Barry Baker ^{3,7},
7 Shobha Kondragunta ⁸, Chuanyu Xu ^{2,8}, Weiwei Chen ⁹, Jeff Mcqueen ¹ and Ivanka Stajner ¹

8 ¹ NOAA/NCEP/Environmental Modeling Center, College Park, MD 20740, USA

9 ² I. M. Systems Group at NOAA, College Park, MD 20740, USA

10 ³ NOAA/OAR/Air Resources Laboratory, College Park, MD 20740, USA

11 ⁴ UMD/Cooperative Institute for Satellite Earth System Studies (CISESS), College Park, MD 20740, USA

12 ⁵ NOAA/OAR/ARL/Atmospheric Turbulence and Diffusion Division, Oak Ridge, TN 37830, USA

13 ⁶ GMU/CISESS, Fairfax, VA 22030, USA

14 ⁷ UMBC/CISESS, Baltimore, MD 21250, USA

15 ⁸ NOAA/NESDIS, College Park, MD 20740, USA

16 ⁹ Northeast Institutes of Geography and Agroecology, Chinese Academy of Sciences, Changchun 130102,
17 P. R. China

18

19 Correspondence to: Li.Pan@noaa.gov

20

21

22

23

24

25 **Abstract**

26 Multiple observation data sets: Interagency Monitoring of Protected Visual Environments
27 (IMPROVE) network data, Automated Smoke Detection and Tracking Algorithm (ASDTA), Hazard Mapping
28 System (HMS) smoke plume shapefiles and aircraft acetonitrile (CH₃CN) measurements from the NOAA
29 Southeast Nexus (SENEX) field campaign are used to evaluate the HMS-BlueSky-SMOKE-CMAQ fire
30 emissions and smoke plume prediction system. A similar configuration is used in the US National Air
31 Quality Forecasting Capability (NAQFC). The system was found to capture most of the observed fire
32 signals. Usage of HMS-detected fire hotspots and smoke plume information were valuable for both
33 deriving fire emissions and forecast evaluation. This study also identified that the operational NAQFC did
34 not include fire contributions through lateral boundary conditions resulting in significant simulation
35 uncertainties. In this study we focused both on system evaluation and evaluation methods. We discussed
36 how to use observational data correctly to retrieve fire signals and synergistically use multiple data sets.
37 We also addressed the limitations of each of the observation data sets and evaluation methods.

38 **Introduction**

39 Wildfires and agricultural/prescribed burns are common in North America all year round, but
40 predominantly occur during the spring and summer months (Wiedinmyer et al., 2006). These fires pose a
41 significant risk to air quality and human health (Delfino et al., 2009; Rappold et al., 2011; Dreessen et al.,
42 2016; Wotawa and Trainer 2000; Sapkota et al., 2005; Jaffe et al., 2013; Johnston et al., 2012). Since
43 January 2015, smoke emissions from fires have been included in the National Air Quality Forecasting
44 Capability (NAQFC) daily PM_{2.5} operational forecast (Lee et al., 2017). The NAQFC fire simulation consists
45 of: the NOAA National Environmental and Satellite Data and Information Service (NESDIS) Hazard
46 Mapping System (HMS) fire detection algorithm, the U.S. Forest Service (USFS) BlueSky-fire emissions
47 estimation algorithm, the U.S. EPA Sparse Matrix operator Kernel Emission (SMOKE) applied for fire plume

48 rise calculations, the NOAA National Weather Service (NWS) North American Multi-scale Model (NAM)
49 for meteorological prediction and the U.S. EPA Community Multi-scale Air Quality Model (CMAQ) for
50 chemical transport and transformation. In contrast to most anthropogenic emissions, smoke emissions
51 from fires are largely uncontrolled, transient and unpredictable. Consequently, it is a challenge for air
52 quality forecasting systems such as NAQFC to describe fire emissions and their impact on air quality
53 (Pavlovic et al., 2016; Lee et al., 2017; Huang et al., 2017).

54 Southeast Nexus (SENEX) was a NOAA field study conducted in the Southeast U.S. in June and July
55 2013 (Warneke et al., 2016). This field experiment investigated the interactions between natural and
56 anthropogenic emissions and their impact on air quality and climate change (Xu et al., 2016; Neuman et
57 al., 2016). In this work, the SENEX dataset was used to evaluate the HMS-BlueSky-SMOKE-CMAQ fire
58 simulations during the campaign period.

59 Two simulations were performed: one with and one without smoke emissions from fires during
60 the SENEX field campaign. Due to the large uncertainties in the estimates of fire emissions and smoke
61 simulations (Baker et al., 2016; Davis et al., 2015; Drury et al., 2014), the first step of the evaluation
62 focused on the fire signal capturing capability of the system. Differences between the two simulations
63 represented the impact of the smoke emissions from fires on the CMAQ model results. Observations from
64 various sources were utilized in this analysis: (i) ground observations (Interagency Monitoring of
65 Protected Visual Environments (IMPROVE)), (ii) satellite retrievals (Automated Smoke Detection and
66 Tracking Algorithm (ASDTA) and HMS smoke plume shape), and (iii) aircraft measurements (SENEX
67 campaign). Fire signals predicted by the modeling system were directly compared to these observations.
68 Several criteria have been used to rank efficacy of the observation systems for fire induced pollution
69 plumes.

70 **Methodology**

71 In this section the NAQFC fire modeling system used in the study was introduced. Uncertainties
72 and limitations in the various modeling components of the system are discussed. Fig. 1 illustrates the
73 schematics of the system. There are four processing steps:

74 **HMS (Hazard Mapping System)**

75 The NOAA NESDIS HMS is a fire smoke detection system based on satellite retrievals. At the time
76 of this study, the satellite constellation used consists of 2 Geostationary Operational Environmental
77 Satellite (GOES-10 and GOES-12) and 5 polar orbiting satellites: MODIS (Moderate-resolution Imaging
78 Spectroradiometer) instruments on NASA EOS -- Terra and Aqua satellites, and AVHRR (Advanced Very
79 High Resolution Radiometer) instruments on NOAA 15/17/18 satellites. HMS detects wildland fire
80 locations and analyzes their sizes, starting times and durations (Ruminski et al., 2008; Schroeder et al.,
81 2008; Ruminski and Kondragunta 2006).

82 HMS first processes satellite data by using automated algorithms for each of the satellite
83 platforms to detect fire locations (Justice et al., 2002; Giglio et al., 2003; Prins and Menzel 1992; Li et al.,
84 2000), which is then manually analyzed by analysts to eliminate false detections and/or add missed fire
85 hotspots. The size of the fire is represented by the number of detecting pixels corresponding to the
86 nominal resolution of MODIS or AVHRR data. Fire starting times and durations are estimated from close
87 inspection of the visible band satellite imagery. A bookkeeping file is generated at the end of this
88 detection step, named "hms.txt" (Fig. 1). It includes all the thermal signal hotspots detected by the
89 aforementioned 7 satellites. During the analyst quality control step, detected potential fire hotspots
90 lacking visible smoke in the retrieval's HMS (RGB real-color) imagery are removed resulting in a reduced
91 fire hotspot file called either "hmshysplit.prelim.txt" or "hmshysplit.txt" to be input into the BlueSky
92 processing step.

93 In general, “hmsysplit.prelim.txt” and “hmsysplit.txt” are very similar, and “hmsysplit.txt” is
94 created later than “hmsysplit.prelim.txt” (Fig. 1). But the differences between “hmx.txt” and
95 “hmsysplit.txt” (“hmsysplit.prelim.txt”) can be rather substantial. The reasons for differences are: 1)
96 many detected fires do not produce detectable smoke; 2) some fires/hotspots are detected only at night,
97 when smoke detection is not possible; 3) smoke emission HMS imagery is obscured by clouds thus not
98 detected by the analyst. Therefore, smoke emission occurrence provided by the HMS is a conservative
99 estimate of fire emissions.

100 By using multiple satellites the likelihood of detecting fires in HMS is robust. However, when the
101 fire geographical size is small the HMS detection accuracy dramatically decreases (Zhang et al., 2011; Hu
102 et al., 2016). Other limitations of the HMS fire detections include ineffective retrievals at nighttime and
103 under cloud cover.

104 **BlueSky**

105 BlueSky, developed by the USFS (US Forest Service), is a modeling framework to simulate smoke
106 impacts on regional air quality (Larkin et al., 2009; Strand et al., 2012). In this study, BlueSky acted as a
107 fire emission model to provide input for SMOKE (Herron-Thorpe et al., 2014; Baker et al., 2016). BlueSky
108 calculates fire emission based on HMS-derived locations (Fig. 1).

109 Fire geographical extent is reflected by the number of nearby fire pixels detected by satellites in
110 a 12-km CMAQ model grid. Fire pixels are converted to fire burning areas in BlueSky based on the
111 assumption that each fire pixel has a size of 1 km² and 10% of its area can be considered as burn-active
112 (Rolph et al., 2009). All fire pixels in a 12-km grid square are aggregated. BlueSky uses the following to
113 estimate biomass availability: fuel loading map is from the US National Fire Danger Rating System (NFDRS)
114 for the Conterminous US (CONUS) with the exception in western US where the HARDY set is used (Hardy
115 and Hardy 2007). BlueSky uses Emissions Production Model (EPM) (Sandberg and Peterson 1984), a simple

116 version of CONSUME, to calculate fuel actually burned -- the so-called consumption sums. Finally, EPM is
117 also used in BlueSky to calculate the fire emission hourly rate per grid-cell. BlueSky outputs CO, CO₂, CH₄,
118 non-methane hydrocarbons (NMHC), total PM, PM_{2.5}, PM₁₀ and heat flux (Fig. 1).

119 BlueSky does not iteratively recalculate fire duration according to the modeled diminishing fuel
120 loading or the modeled fire behavior. In the aggregation process, when there is more than one HMS point
121 in a grid cell which have different durations, all points in that grid cell would be assigned the largest
122 duration in all points. For an example, if there were 3 HMS points that had durations of 10, 10 and 24
123 hours, the aggregation would include 3 points (representing 3 km²) assigned with 24 hour duration to all
124 of the 3 HMS points.

125 HMS has no information about fuel loading. BlueSky uses a default fuel loading climatology over
126 the eastern US. BlueSky uses an idealized diurnal profile for fire emissions. Uncertainties in fire sizes, fuel
127 loading and fire emission rates lead to large uncertainties in wildland smoke emissions (Knorr et al., 2012;
128 Drury et al., 2014; Davis et al., 2015).

129 **SMOKE**

130 In SMOKE (Sparse Matrix Operator Kernel Emission), the BlueSky fire emissions data in a
131 longitude-latitude map projection are converted to CMAQ ready gridded emission files (Fig. 1). Fire smoke
132 plume rise is calculated using formulas by Briggs. The heat flux from BlueSky and NAM meteorological
133 state variables are used as input (Erbrink 1994). The Briggs' algorithm calculates plume top and plume
134 bottom, between plume top and bottom the emission fraction is calculated layer by layer assuming a
135 linear distribution of flux strength in atmospheric pressure. For model layers below the plume bottom the
136 emission fraction is assumed to be entirely in the smoldering condition as a function of the fire burning
137 area.

138 A speciation cross-reference map was adopted to match BlueSky chemical species to that in
139 CMAQ using the U.S. EPA Source Classification Codes (SCCs) for forest Wildfires
140 (<https://ofmpub.epa.gov/scsearch/docs/SCC-IntroToSCCs.pdf>). The life-span of fire is based on the HMS
141 detected fire starting time and duration. During fire burning hours a constant emission rate is assumed.
142 This constant burn-rate has been shown to be a crude estimate (Saide et al., 2015; Alvarado et al., 2015).
143 Other uncertainties include plume rise (Sofiev et al., 2012; Urbanski et al., 2014; Achtemeier et al., 2011)
144 and fire-weather (fire influencing local weather).

145 **CMAQ**

146 The CMAQ version 4.7.1 was used. The CB05 gas phase chemical mechanism (Yarwood et al.,
147 2005) and the AERO5 aerosol module (Carlton et al., 2010) were chosen. Anthropogenic emissions were
148 based on the U.S. EPA 2005 National Emission Inventory (NEI) projected to 2013 (Pan et al., 2014),
149 Biogenic emissions (BEIS 3.14) were calculated in-line inside CMAQ.

150 **Simulations**

151 The NAM provided meteorology fields to drive CMAQ (Chai et al., 2013). NAM meteorology is
152 evaluated daily and results (BIAS and RMSE etc.) are posted on:
153 “<http://www.emc.ncep.noaa.gov/mmb/mmbpll/mmbverif/>”. The simulation domain is shown in Fig. 1. It
154 includes two domains: (i) a 12-km domain covering the Continental U.S. (CONUS); and (ii) a 4km domain
155 covering the Southeast U. S. where the majority of SENEX measurements occurred. Lateral boundary
156 conditions (LBC) used in the smaller SENEX domain simulation were extracted from that from the CONUS
157 simulations. Four scenarios were simulated: CONUS with fire emissions, CONUS without fire emissions,
158 SENEX with fire emissions and SENEX without fire emissions.

159 There were several differences in system configuration between the NAQFC fire smoke
160 forecasting and the “with-fire” simulation in this study. For models, the BlueSky versions used in NAQFC

161 and that in this study are v3.5.1 and v2.5, respectively; CMAQ versions used in NAQFC and in this study
162 are v5.0.2 and v4.7.1, respectively. For simulations, current fire smoke forecasting in the NAQFC includes
163 two runs: the analysis and the forecast (Huang et al. 2019 (manuscript in preparation)). The analytical run
164 is a 24-hour retrospective simulation using yesterday's meteorology and fire emissions to provide initial
165 conditions for today's forecast. The forecasting run is a 48-hour predictive simulation using yesterday's
166 fire emissions, assuming fires with duration of more than 24 hours are projected as continued fires.. The
167 "with-fire" simulation in this study is exactly identical to the analysis run in NAQFC.

168 **Evaluations**

169 Carbon monoxide (CO) has a relatively long life time in the air and is emitted by biomass burning.
170 CO was used as a fire tracer in the prediction. The CO difference (ΔCO) between CMAQ simulations with
171 and without fire emissions was used as the indicator of fire influence. For additional observations
172 included: potassium (K) collected at the IMPROVE (Interagency Monitoring of Protected Visual
173 Environments) sites within the SENEX domain; acetonitrile (CH_3CN) measured from the SENEX campaign
174 flights; and fire plume shape detected by the HMS analysis as real fire signals. The enhancement in ΔCO
175 concentration due to fire was directly compared with those signals. At the same time, ΔAOD (Aerosol
176 Optical Depth) from CMAQ ("with-fire" simulated concentration minus that with "without-fire") was also
177 used as fire indicator when compared with smoke masks given by the ASDTA (Automated Smoke
178 Detection and Tracking Algorithm).

179 It is almost impossible to assess the uncertainty of each specific smoke physical process. In each
180 modeling step in HMS, BlueSky, SMOKE and CMAQ, the modeling system accrues uncertainties. Such
181 uncertainties were likely cumulative and might lead to larger error in succeeding components
182 (Wiedinmyer et al., 2011). For an example, heat flux from BlueSky influenced plume rise height in SMOKE
183 and consequently influenced plume transport in CMAQ. It is also noteworthy that when modeled ΔCO

184 was against measured K or CH₃CN, the objective was to search for enhancement signals resulting from
185 fires but not aiming to account for proportional concentration changes in the tracers in the event of a fire.
186 Attempting to account for CMAQ simulation uncertainties in surface ozone and particulate matter as a
187 function of smoke emissions from fires was difficult. Neither was it the objective of this study. Rather,
188 the purpose of this study is to focus on analyzing the capability of the HMS-BlueSky-SMOKE-CMAQ
189 modeling system to capture fire signals.

190 The SENEX campaign occurred in June and July and our model simulations were from June 10 to
191 July 20, 2013. Throughout the campaign all available observation datasets were used including ground-,
192 air- and satellite-based acquired data. Each dataset had its unique characteristics and linking them
193 together gave an overall evaluation. At the same time, in each dataset our evaluations included as many
194 as possible observed fire cases. Both well-predicted and poorly-predicted cases are presented to illustrate
195 potential reasons responsible for the modeling system's behavior.

196 **Results and Discussions**

197 **Observed CO versus modeled CO in SENEX**

198 Table 1 lists observed and modeled CO vertical profiles for the "with-fire" and "without-fire" cases
199 during the SENEX campaign. Observed CO concentrations between the surface and 7 km AGL (Altitude
200 above Ground Level) in the SENEX domain area remained greater than 100 ppb during all 40 days of the
201 campaign. The highest CO concentrations were measured closer to the surface. The maximum measured
202 CO concentration of 1277 ppb was observed during a flight on July 03 at an ASL (Altitude above Sea Level)
203 of 974 m. In this flight strong fire signals were observed but the fire simulation system missed those signals
204 as discussed below.

205 CO concentrations were underestimated by the model in almost all cases even when the model
206 captured CO contribution from fire emissions spatio-temporarily. Mean ΔCO in each height interval was
207 usually above 1.5 ppb but less than 2.0 ppb. Fig. 2a shows the contribution of total CO emissions from
208 fires which occurred inside the SENEX domain over the simulation period. The maximum CO emissions
209 contribution from fires was about 3% during the campaign. In most of those days fire emission
210 contributions in SENEX were less than 1%. The averaged contribution during those 40 days was 0.7%. Fig.
211 2b shows the contribution of CO flowing into the SENEX domain from its boundary caused by fire outside
212 the SENEX domain but inside the CONUS domain (Fig. 1). The averaged fire contribution to CO from
213 outside the SENEX domain was 0.67%. CO influenced by fire emission in June is greater than that in July.

214 During the field experiment the general lack of large fires made evaluation of modeled fire
215 signature difficult since it was easier to capture large fire signals than the smaller fires. We postulated that
216 a clear fire signal simulated in the HMS-BlueSky-SMOKE-CMAQ system could be indicated by ΔCO
217 significantly larger than its temporal averages resulted by fires originated from inside and/or outside the
218 SENEX domain. For an example, a clear fire signal between 500 m and 1000 m AGL was indicated by ΔCO
219 across those altitudes and when the concentration of ΔCO was above 2.0 ppb based on the campaign
220 duration averaged CO concentration of about 150 ppb as well as on within the SENEX domain and outside
221 of the SENEX domain fire contributions to CO ($150 \times (0.007 + 0.0067) = 2.0$).

222 Figure 3 displays the simulated ΔCO extracted along a SENEX flight path. The modeled
223 concentration showed that the fire impacts on SENEX were not negligible despite a lack of larger fire
224 events as shown in Fig. 2a and 2b during the SENEX campaign period. That confirmed the importance of
225 evaluating the fire simulation system in an air quality model. Unless a model is able to predict fire signals
226 correctly it is useless for modelers to discuss fire effects on chemical composition of the atmosphere. A

227 detail of how model caught or missed or falsely predicted fire signals during the SENEX campaign and a
228 comparison of ΔCO versus CH_3CN will be discussed in the follow discussion.

229 **IMPROVE**

230 The Interagency Monitoring of Protected Visual Environments (IMPROVE) is a long term air
231 visibility monitoring program initiated in 1985 (<http://vista.cira.colostate.edu/Improve/data-page>). It
232 provides 24-h integrated particulate matter (PM) speciation measurements every third day (Malm et al.,
233 2004; Eatough et al., 1996). The IMPROVE dataset was chosen for this analysis because it included K
234 (potassium), OC (organic carbon) and EC (elemental carbon), important fire tracers. IMPROVE monitors
235 are ground observation sites likely influenced by nearby fire sources.

236 There were 14 IMPROVE sites in the SENEX domain (Fig. 4). Potential fire signals were identified
237 by using CMAQ modeled ΔCO and IMPROVE observed K. However, in addition to fires K has multiple
238 sources such as soil, sea salt and industry. Co-incidentally fires should also produce enhanced EC and OC
239 concentrations, a fire signal should reflect above-average values for EC, OC, and K. EC, OC and K
240 observations that were 20% above their temporal averages during the SENEX campaign were used as a
241 predictor for fire event identification. Meanwhile, co-measured NO_3^- and SO_4^{2-} concentrations is less than
242 1.5 times of their respective temporal averages for screening out data with industrial influences. Lastly, a
243 third predictor was employed so that concentrations of other soil components besides K should be below
244 their temporal average to eliminate conditions of spikes in K concentration due to dust. With these three
245 criteria the IMPROVE data was screened for fire events (See Table 2).

246 Five fire events were observed at four IMPROVE sites. Table 2 lists measured EC, OC, NO_3^- , K, soil
247 and SO_4^{2-} concentrations ($\mu\text{g m}^{-3}$) and their ratios to averages. BC versus OC and K versus BC ratios were
248 also calculated and listed in Table 2 to illustrate the application of our criteria. It was found that except
249 for monitor BRIS, all other sites (COHU, MACA and GRSM) had BC/OC and K/BC ratios comparable to the

250 ratios of the same quantities due to biomass burning reported by other researchers (Reid et al., 2005;
251 DeBell et al., 2004). BRIS is a coastal site likely influenced by sea salts (Fig. 4).

252 For the four identified fire cases, ΔCO as a modeled fire tracer around the IMPROVE site was
253 plotted. Fire signals on June 21 at COHU and GRSM and on June 24 at MACA were reproduced in model
254 simulation. The June 24 MACA case was used as an example (see Fig. 4). On June 24, 2013, detected fire
255 spots were outside the SENEX domain, but SSW wind blew smoke plumes into the SENEX domain and
256 affected modeled CO in MACA. Modeled ΔCO in MACA was 5 ppb.

257 Another IMPROVE site located upwind of MACA, CADI, was also potentially under the influence
258 of that fire event; however, data from CADI on June 24 did not indicate a fire influence, possibly due to
259 the frequency of IMPROVE sampling that eluded measurement or that the smoke plume was transported
260 above the surface in disagreement with what was modeled. Within the four fire cases identified by the
261 IMPROVE data during SENEX (Tab. 2), the model successfully captured three out of four events. The model
262 missed fire signal on July 3 at MACA. The model missed the fire signal on July 3 at MACA. The following
263 section is dedicated to the July 3 SENEX flight.

264 **Plume Spatial Coverage**

265 HMS determines fire hotspot locations associated with smoke and upon incorporating the smoke
266 plume shape information from visible satellite images. HMS provides smoke plume shapefiles over much
267 of North America, which is a two-dimensional smoke plume spatial depiction collapsing all plume
268 stratifications to a satellite eye-view. For modeled plumes, we integrated modeled ΔCO by multiplying the
269 layer values with the corresponding CMAQ model layer thicknesses and air density to derive a simulated
270 smoke plume shape. HMS-derived smoke plume shape versus CMAQ predicted smoke plume shape was
271 then used to evaluate the fire simulation.

272 Figure of Merits in Space (FMS) (Rolph et al., 2009) is a statistic for spatial analysis and was
273 calculated as follows:

$$274 \quad \text{FMS} = \frac{\text{Area}_{\text{hms}} \cap \text{Area}_{\text{cmaq}}}{\text{Area}_{\text{hms}} \cup \text{Area}_{\text{cmaq}}} \times 100\%$$

275 Where Area_hms represents area of grid cells influenced by fire emission over CONUS detected by HMS
276 and Area_cmaq represents area of grid cells over CONUS identified by model prediction. In general, a
277 higher FMS value indicates a better agreement between the observed and modeled plume shape (Rolph
278 et al., 2009).

279 Figure 5 summarizes FMS during the SENEX campaign. Average FMS was 22% with its maximum
280 at 56% on July 6 and minimum at 1.2% on June 17 2013. Figure 6a exhibits HMS detected smoke plume
281 and CMAQ calculated smoke plume over CONUS on July 6. The FMS score was 56% meaning that the
282 modeled plume shape was consistent with that of HMS. However, HMS-BlueSky-Smoke emissions system
283 might have underestimated the intensive fire influence areas along the border of California and Nevada.
284 Subsequently, the model also under-predicted its associated influence in North Dakota, South Dakota,
285 Minnesota, Iowa and Wisconsin.

286 Figure 6b exhibits the worst case on June 17 2013 in terms of resulting with a FMS score at 1.2%.
287 Two reasons led to this: (i) CMAQ missed fire emissions from Canada. Those fire sources located outside
288 the CONUS modeling domain and our simulation system used a climatologically-based static LBC; Secondly
289 on June 17, there were a lot of fire hotspots in the Southeastern U.S., i.e., in Louisiana, Arkansas and
290 Mississippi along the Mississippi River. Hotspots were detected but they lacked associated smoke in
291 corresponding HMS imagery (Fig. 6c). This could be due to cloud blockage or to small agricultural debris
292 clearing, burns in under-bushes or prescribed burns. These conditions prevented the HMS from
293 identifying fires and hence emissions were not modeled for those sources.

294 It is noteworthy that the FMS evaluation contained uncertainties contributed from both modeled
295 and observed values. The calculated campaign duration and SENEX-wide averaged FMS was 22%. It is
296 significantly higher than that achieved by similar analyses done by HYSPLIT (Hybrid Single Particle
297 Lagrangian Integrated Trajectory) smoke forecasting for the fire season of 2007 (6.1% to 11.6%) (Rolph et
298 al., 2009). The primary reason is that the HYSPLIT smoke simulation is accessed at the invocation of a
299 forecast cycle the HMS fire information which is already one day old due to retrieval latency and cycle-
300 queuing issues. However, our model simulation in this study was from a retrospective module using
301 current day HMS fire information. Such discrepancies have been discussed by Huang et al. 2019
302 (*manuscript in preparation*). The secondary reason is plume rise: despite both the HYSPLIT and CMAQ fire
303 plume rise were estimated by the Briggs' equation, the HYSPLIT plume rise was limited to 75% of the
304 mixed layer height (MLH) at daytime and two times MLH at nighttime, whereas the CMAQ fire plume rise
305 did not have these limitations.

306 **ASDTA**

307 The Automated Smoke Detection and Tracking Algorithm (ASDTA) is a combination of two data
308 sets: (1) the NOAA Geostationary satellite (G13) retrieves thermal enhancements aerosol optical depth
309 due to fires using visible channels and produces a product called GOES Aerosol/Smoke Product (GASP)
310 (Prados et al., 2007); and, (2) NOAA NESDIS HMS (Hazard Mapping System) fire smoke detection. First,
311 the observation of the increase in AOD near the fire is attributed to the specific HMS fire; AOD
312 values not associated with fires are dropped. Second, a pattern recognition scheme uses 30-
313 minutes geostationary satellite AOD images to tracks the transport of this smoke plume away
314 from the source. ASDTA provides the capability to determine whether the GASP is influenced by one or
315 multiple smoke plumes over a location at a certain time.

316 ASDTA is originally generate to provide operational support for verification of the NOAA HYSPLIT
317 dispersion model predicts smoke plume direction and extension (Draxler and Hess 1998). These data are
318 also suitable for model performance evaluation in this study. For each simulation, modeled AOD was
319 calculated for each sensitivity test (“with-fire” or “without-fire”) and Δ AOD is defined as the difference
320 obtained by subtracting AOD_without-fire from AOD_with-fire.

321 Figure 7a illustrates a GOES retrieved AOD (summed over from 10:00 am to 2:00 pm at local time)
322 contour plot that reflects influences by smoke plumes over the CONUS domain on June 14 2013. Figure
323 7b presents similar results, but for simulated Δ AOD (with-fire – without-fire). For further evaluation of
324 the HMS detected smoke plume shape Fig. 7c can be compared with Figs. 7a and 7b. Figure 7a shows
325 several regions under the influence of fires in: California, northwest Mexico, Kansas, Missouri, Oklahoma,
326 Arkansas, Texas and part of the Gulf of Mexico. In the northeastern USA, fire plumes occurred
327 occasionally. Those regions agreed relatively well with the shaded contours between Figs. 7a and 7c.
328 However, due to the lack of fire treatments in the CMAQ LBC, the simulation (Fig. 7b) missed smoke
329 influence on the northeast region of the CONUS domain. CMAQ also failed to simulate the fire influences
330 in the southwest region of the domain.

331 Similar plots for June 25 are shown in Figs. 7d, 7e and 7f for ASDTA, CMAQ and HMS, respectively.
332 The ASDTA (Fig. 7d) diagnosed an overestimation in fire influences in the south including Texas and the
333 Gulf of Mexico and an underestimation in the northeastern U.S. On the other hand, the model predicted
334 two strong fire signals clearly: near the border between Arizona and Mexico, and in Colorado (See Fig. 7e).
335 All the fire influenced areas in Fig. 7e were seen in observation by HMS in Fig. 7f.

336 Comparing ASDTA plots and CMAQ Δ AOD plots (Fig. 7a vs 7b; Fig. 7d vs 7e), both similarities and
337 differences were found. Similarities were attributable to similar fire accounting and meteorology.
338 Differences were attributable to: HMS contains more fire hotspots than those used by CMAQ due to

339 domain size; only fires inside the CONUS were included in the CMAQ fire simulation and LBCs did not vary
340 to reproduce impacts of wildfires from outside of the domain.

341 **SENEX**

342 SENEX (Southeast Nexus) was a field campaign conducted by NOAA in cooperation with the US
343 EPA and the National Science Foundation in June and July 2013. Although SENEX was not specifically
344 designed for fire studies, its airborne measurements included PM_{2.5} OC and EC, CO and acetonitrile
345 (CH₃CN). CH₃CN was chosen as a fire tracer since it is predominantly emitted from biomass burning
346 (Holzinger et al., 1999; Singh et al., 2012).

347 CH₃CN has a residence time in the atmosphere of around 6 months (Hamm and Warneck 1990)
348 and the reported CH₃CN background concentration is around 100 - 200 ppt (Singh et al., 2003). Measured
349 CH₃CN concentrations tend to increase with altitude (Singh et al., 2003; de Gouw et al., 2003), since
350 biomass burning plumes tend to ascend during long-range transport. During SENEX, measured CH₃CN
351 showed a similar pattern. Fire signals were identified through airborne measurements of CH₃CN when its
352 concentration exceeded the background; e.g., on July 3 2013, or when its concentration peak appeared
353 at high altitude; e.g., on June 16 2013 and July 10 2013.

354 CH₃CN airborne measurements were used to identify fire plumes at certain locations and heights
355 during SENEX. For model evaluations, fire locations and accurate meteorological wind field are crucial to
356 interpret 2-D measurements such as IMPROVE, HMS and ASDTA. To verify a 3-D fire field, it is critical to
357 capture plume rise. However, it was extremely difficult to back out plume rise from the airborne
358 measurements. An additional uncertainty arose in the difference of temporal resolutions of the data:
359 IMPROVE, HMS shapefiles and ASDTA were daily or hourly data, whereas airborne CH₃CN data were
360 measured at one-minute intervals.

361 Figure 8a shows a CMAQ simulated ΔCO vertical distribution along flight transects on June 16
362 2013. This flight occurred during the weekend over and around power plants around Atlanta, GA. The
363 color of flight path represents observed CH_3CN concentration in ppt. In Fig. 8a, the concentration of ΔCO
364 increased from surface to 5000 m, especially above 2000 m. Six CH_3CN concentration peaks were observed
365 when AGL was above 2500 m.

366 For CMAQ simulated ΔCO , five out of six fire signals detected by CH_3CN measured spikes were
367 captured where ΔCO concentrations were all above 3 ppb. Only one fire signal was missed by the model
368 at 18:30 UTC June 16 2013. Model simulation showed that long range transports (LRT) of smoke plumes
369 influenced airborne observations. Fire signals from the free troposphere subsided and influenced flight
370 measurements. High EC or OC or CO did not concur with high CH_3CN observation probably due to species
371 lifetime differences. HMS smoke plume did not show any hotspots or smoke plume around Atlanta
372 suggesting that the sources of those observed fire signals were not from its vicinity.

373 A similar phenomenon was seen in SENEX flight 0710, which occurred during flight transects from
374 Tennessee to Tampa, FL. Figure 8b is a similar graph as Fig. 8a. Based on ΔCO concentrations, CMAQ
375 captured the July 10 case as fire signals were observed. Nonetheless, ΔCO may be over predicted at
376 around 19 UTC. The model exhibited a fire signal with ΔCO concentration of about 3 ppb near 6000 m
377 around 19 UTC, whereas measured CH_3CN was 120 ppt.

378 **SENEX flight on July 3**

379 Observations from IMPROVE, HMS and SENEX identified fire signals on July 3 2013. ASDTA
380 retrievals were not available. Those signals were missed by the model. In this section, all of evaluation
381 methods addressed above were used to study potential causes of failure of the model to reproduce fire
382 signals.

383 At the MACA IMPROVE site on July 3 2013, the wind direction at the surface was southeasterly,
384 with no fire hotspots (solid black circle) located upwind of MACA (Fig. 9a). Without any identified hotspots
385 upwind, the model missed fire signals observed at MACA on July 3 2013.

386 Flight #0703 was a night mission targeting power plants in Missouri and Arkansas. The flight path
387 is shown in Fig. 9b and is colored by measured CH_3CN concentration. In order to highlight CH_3CN
388 concentrations above 400 ppt in the measurements, CH_3CN concentrations below 400 ppt were
389 represented by black dots. During the flight, 16 measurements of acetonitrile concentration above 400
390 ppt were observed and the maximum was 3227.9 ppt. These observations were located over
391 northwestern Tennessee and close to the borders of Kentucky, Illinois, Missouri and Arkansas. Except for
392 one observation, the flight ASL was between 500 m and 1000 m.

393 Enhancements of CO and OC were also measured concurrently with CH_3CN . Figures 9c and 9d
394 show scatter plots for CH_3CN versus CO and OC, respectively. Measured CH_3CN was highly correlated to
395 both measured CO and OC, with linear correlation coefficients (R^2) of 0.83 and 0.71, respectively. The
396 $\Delta\text{CH}_3\text{CN}/\Delta\text{CO}$ ratio is around 2.7 (ppt/ppb), which is consistent with findings of other measurements over
397 California in 2002 when a strong forest fire signal was intercepted by aircraft (de Gouw et al., 2003). The
398 $\Delta\text{CH}_3\text{CN}/\Delta\text{OC}$ ratio was around 6.85 (ppt/(mg m^{-3})), which is also in the range of biomass burning analyses
399 in MILAGRO (Megacity Initiative Local and Global Research Observations) (Aiken et al., 2010).

400 Figure 9e shows model simulated ΔCO with peaks at AGL below 3000 m. Fire signals showed
401 substantial influences on aircraft measurement at around 5 UTC. However, clear fire signals between 2
402 UTC and 3 UTC were observed based on prior CH_3CN analysis. The model either predicted insufficient fire
403 emission influences or missed it. FMS score on July 3 was 30%. Figure 9f shows that CMAQ did not predict
404 plumes where the HMS plume analysis exhibited several dense smoke plumes. As NOAA Smoke Text
405 Product (<http://www.ssd.noaa.gov/PS/FIRE/DATA/SMOKE>) described on its July 03 0501 UTC report: a

406 smaller very dense patch of remnant smoke, analyzed earlier the same day over southern Missouri, drifted
407 southward into Arkansas.”

408 The reasons the model missed these fire observations were not clear. Figures 10, 11a and 11b
409 suggest a few clues. Figure 10 is a backward trajectory analysis plot for the observations obtained during
410 the SENEX flight on July 3 with CH₃CN measured concentration above 400 ppt. Both transect and passing
411 altitude of the air parcels clearly showed those measurements were most likely influenced by the nearby
412 pollution sources. Figure 11a illustrates the locations of fire used in the CMAQ simulation. It is noted that
413 hmsysplit.txt is input into BlueSky after HMS quality control (Fig. 1). There were several hotspots around
414 the region where the IMPROVE site MACA was located and where the SENEX flight overpassed. Our fire
415 simulation system might have underestimated smoke emissions from those fires. Other explanation was
416 from Fig. 11b, which illustrated hotspots in hmx.txt. In hmx.txt, every detected fire spots by HMS before
417 quality control were showed. Comparing Fig. 11a with 11b, there were clusters of fire spots in the central
418 U. S. especially in West Tennessee. However, those spots were removed during the HMS quality control
419 process because there were no associated smoke plumes visible. In most of times, those fires were
420 believed to be small sized fires such as from agriculture fires or prescribed burns. For this case, there seem
421 to have been thin clouds overhead and thicker clouds in the vicinity,
422 (<http://inventory.ssec.wisc.edu/inventory/image.php?sat=GOES-13&date=2013-07>
423 [03&time=16:02&type=Imager&band=1&thefilename=goes13.2013.184.160147.INDX&coverage=CONUS](http://inventory.ssec.wisc.edu/inventory/image.php?sat=GOES-13&date=2013-07-03&time=16:02&type=Imager&band=1&thefilename=goes13.2013.184.160147.INDX&coverage=CONUS)
424 [&count=1&offsetz=0](http://inventory.ssec.wisc.edu/inventory/image.php?sat=GOES-13&date=2013-07-03&time=16:02&type=Imager&band=1&thefilename=goes13.2013.184.160147.INDX&coverage=CONUS&count=1&offsetz=0)), so it would be hard to differentiate smoke from clouds by satellite observations

425 **CONCLUSIONS**

426 In support of the NOAA SENEX field experiment in June-July 2013, simulations were conducted
427 including smoke emissions from fires. In this study, a system accounting for fire emissions in a chemical

428 transport model is described, including a satellite fire detecting system (HMS), a fire emission calculation
429 model (BlueSky), a pre-processing of fire emissions (SMOKE), and simulation over the SENEX domain by
430 CMAQ. The focus of this work is to evaluate the system's capability to capture fire signals identified by
431 multiple observation data sets. These data sets included IMPROVE ground station observations, satellite
432 observations (HMS plume shapefile and ASDTA) and airborne measurements from the SENEX campaign.

433 For IMPROVE data, potential fire signals were identified by measured potassium concentrations
434 in $PM_{2.5}$. Fire identifications in CMAQ rely on predicted ΔCO , the difference between simulations with and
435 without fire emissions. Three out of four observed fire signals were captured by CMAQ simulations. For
436 HMS smoke plume shapefiles that were manually plotted by analysts to represent the regions impacted
437 by smoke, we used FMS to calculate the percentage of its overlapping with CMAQ predicted smoke
438 plumes. FMS averaged 22% over forty days of the SENEX campaign. In terms of fire smoke impacts on
439 ΔAOD , both ASDTA and CMAQ showed patterns that were compared to HMS plume shapefile. In terms of
440 measured CH_3CN , a biomass burning plume tracer, both SENEX aircraft in-flight measurements and CMAQ
441 simulations captured signatures of long range transport of fire emissions from elsewhere in the CONUS
442 domain.

443 Generally, using HMS-detected fire hotspots and smoke data was useful for predictions of fire
444 impacts and their evaluation. The HMS-BlueSky-SMOKE-CMAQ fire simulation system, which is also used
445 in NAQFC, was able to capture most of the fire signals detected by multiple observations. However, the
446 system failed to identify fire cases on June 17 and July 3 2013 -- thereby demonstrating two problems
447 with the simulation system. One identified problem was the lack of a dynamical fire LBC bounding the
448 CONUS domain to represent the inflows of strong fire signals originating from outside the simulation
449 domain. Secondly, the HMS quality control procedure eliminated fire hotspots that were not associated
450 with visible smoke plumes leading to an underestimation.

451 We were keen on understanding and quantifying the various uncertainties and observational
452 constraints of this study therefore the following rules of thumb were observed: (1) a holistic evaluation
453 approach was adopted so that the fire smoke algorithm was interpreted as a single entity to avoid
454 deadlock due to over-interpretation of uncertainty of the single component in the system; (2) analysis
455 conclusion applicable to the entire simulation period was drawn so that the episodic characteristics of the
456 cases embedded in the simulation were averaged and generalized. This new methodology may benefit
457 NAQFC; (3) we took advantage of the multiple perspectives of the observation systems that offered a wide
458 spectrum of temporal and spatial variabilities intrinsic to the systems; (4) we were intentionally
459 conservative in discarding data so that we maximized the sampling pool for statistical analysis and avoided
460 unwittingly discarding poorly simulated cases, good outliers, and weak but accurate signals.

461 Quantitative evaluation of fire emissions and their subsequent influences on ozone and
462 particulate matter in this fire and smoke prediction system is challenging. Future work includes applying
463 these findings to the NAQFC and improving the NAQFC system's capabilities to simulate fires accurately.

464 **Code Availability**

465 The source code used in this study is available online at
466 <http://www.nco.ncep.noaa.gov/pmb/codes/nwprod/cmaq.v5.0.2>.

467 **Acknowledgements & disclaimer**

468 This work was partially funded by the NASA Air Quality Applied Sciences Team (AQAST), project
469 grant NNH14AX881. The authors are thankful to Dr. Joost De Gouw and Dr. Martin G. Graus of the Earth
470 System Research Laboratory, NOAA for sharing the SENEX campaign data used in this study. Although this
471 work has been reviewed by the Air Resources Laboratory, NOAA and approved for publication it does not
472 necessarily reflect their policies or views.

473 **Figures:**

474 Figure 1, Fire emission calculation and smoke plume simulation algorithm.

475 Figure 2, in 4km SENEX domain, (a): the contribution (%) of CO emission from fires occurred inside the
476 SENEX domain; (b): the contribution (%) of CO flux flowing into the SENEX domain from its boundary
477 caused by fires burning outside the SENEX domain but inside the CONUS domain.

478 Figure 3, simulated ΔCO (ppb) extracted along SENEX flight path.

479 Figure 4, ΔCO (>2.0 ppb) simulated in SENEX domain on June 24 2013. The solid circle is detected fire
480 hotspots by HMS. The open triangle represents IMPROVE sites.

481 Figure 5, FMS (Figure of Merits in Space) (%) from June 11 to July 19 in 2013 during SENEX experiment.

482 Figure 6, HMS observed plume shape versus CMAQ predicted plume shape on (a): July 6 2013; (b): June
483 17 2013; The light blue shading represents modeled plume shape (defined as total column ΔCO) and the
484 thin dash line and emboldened green lines encircle areas representing HMS-derived light and strong
485 influenced plume shape, respectively. (c): HMS observed fire hotspots (red) and plume shapes (white)
486 (<http://ready.arl.noaa.gov/data/archives/fires/national/arcweb>) on June 17, 2013.

487 Figures 7, GOES detected AOD influenced by fires using ASDTA diagnose method. Color-shaded region
488 represents the fire-smoke influenced areas and the color denotes the magnitude of the retrieved AOD on
489 (a): June 14 2013; (d): June 25 2013; ΔAOD (with-fire – without-fire) simulated in CMAQ on (b): June 14
490 2013; (e): June 25 2013; HMS observed fire hotspots (red) and plume shapes (white)
491 (<http://ready.arl.noaa.gov/data/archives/fires/national/arcweb>) on (c): June 14 2013; (f): June 25 2013.

492 Figure 8, CMAQ simulated ΔCO vertical distributions along SENEX flight transect on (a): June 16 2013; (b):
493 July 10 2013; The x-axis label is UTC (hour) and the y-axis label is AGL (m). Two color bars represent
494 observed CH_3CN concentration (rectangle bar in ppt) and simulated ΔCO concentration (fan bar in ppb),
495 respectively.

496 Figure 9, plots for July 3 2013 case, (a): IMPROVE; (b): the flight path of SENEX #0703 colored by measured
497 CH_3CN concentration (ppt); (c): CH_3CN (ppt) vs CO (ppb); (d): CH_3CN (ppt) vs AMS_Org (mg m^{-3}); (e): CMAQ
498 simulated ΔCO vertical distributions along flight transect; (f): HMS observed plume shape versus CMAQ
499 prediction.

500 Figure 10, a backward trajectory analysis for the observations obtained during the SENEX flight on July
501 03 2013 with CH_3CN measured concentration above 400 ppt.

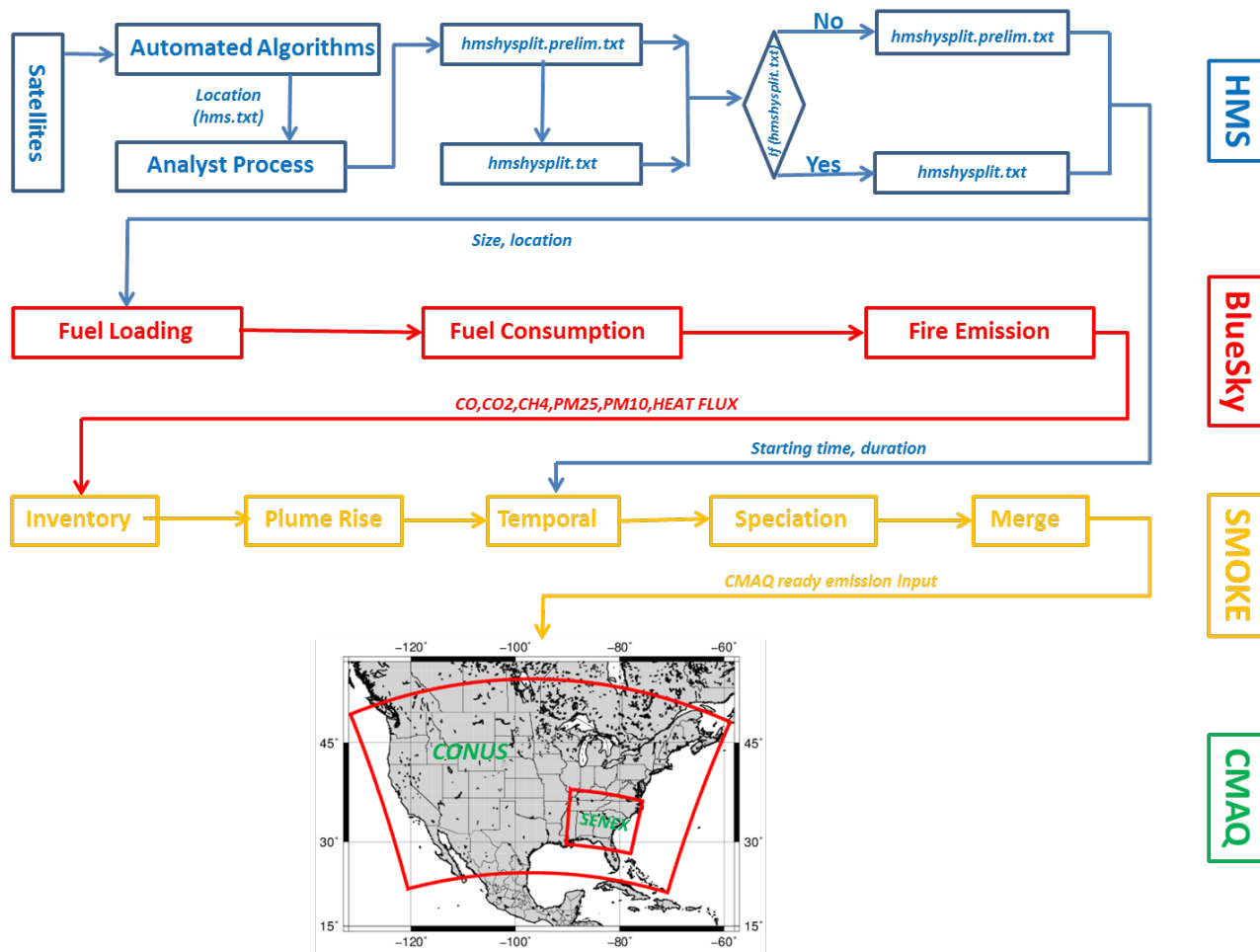
502 Figure 11, detected fire hotspots on July 03 2013 (a): hmxhysplit.txt; (b): hmx.txt.

503

504

505

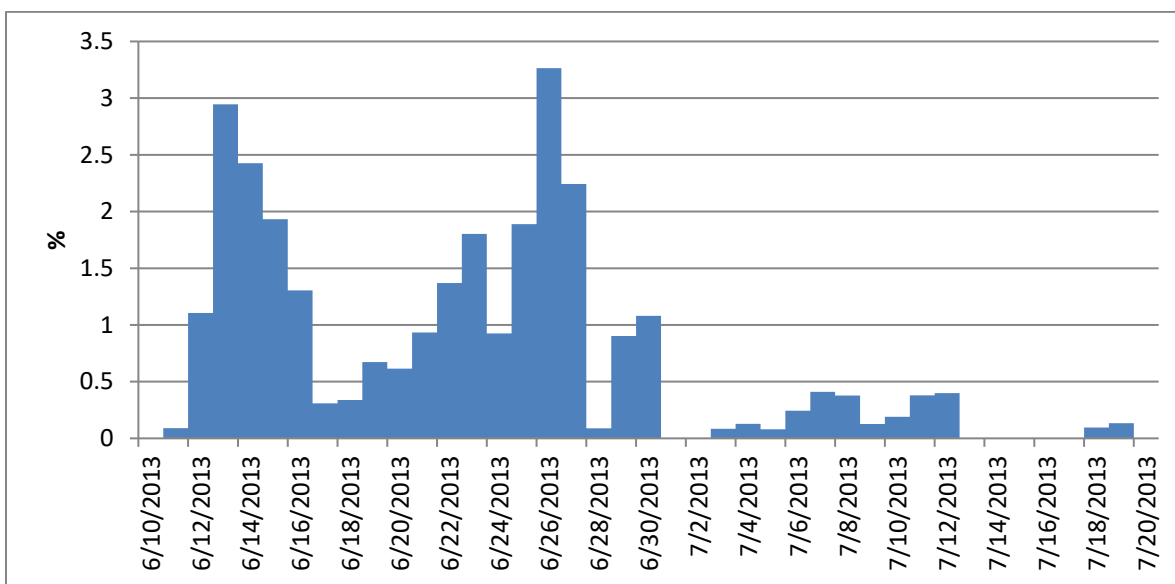
506
507
508
509



510
511
512
513
514
515
516
517
518
519

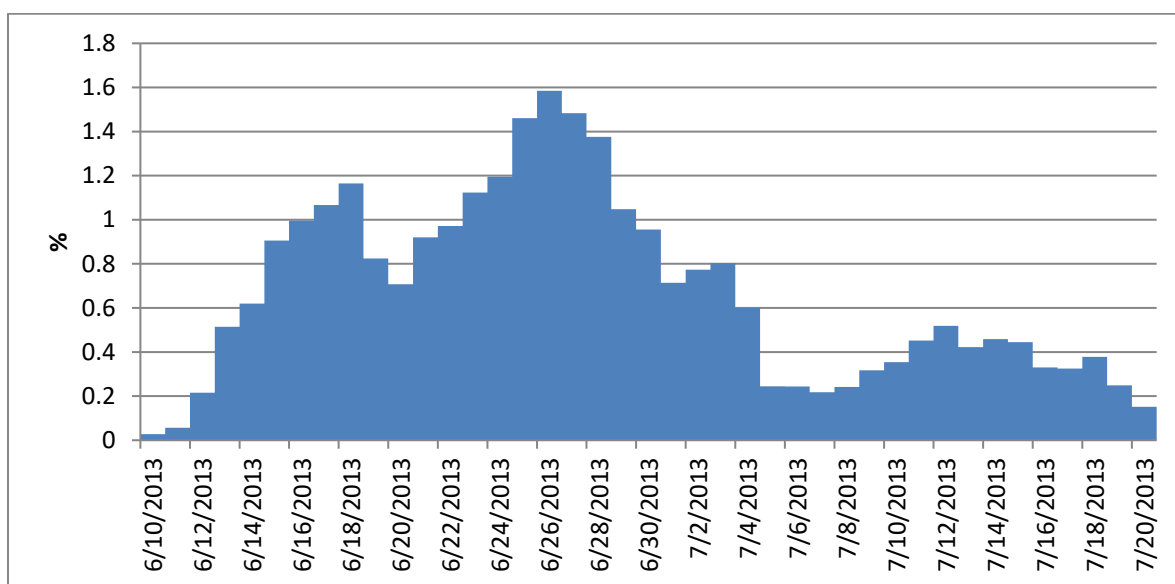
Figure 1: Schematics of fire emission and smoke plume simulation system used: Data-feed and/or modeling of physical and chemical processes were handled largely sequentially from top to bottom and from left to right; The right hand four vertical boxes depict the submodel names: NESDIS Hazard Mapping System (HMS) for wild fire hot spot detection; US Forest Service’s Bluesky for fuel type and loading parameterization; and US EPA’s Sparse Matrix Operator Kernel (SMOKE) to handle emission characterization; and lastly the Community Multiple-scale Air Quality model (CMAQ) was applied to simulate the transformation, transport and depositions of the atmospheric constituents. The “SENEX” in-set framed by red emboldened lines was the domain for this study.

520



521

522 **Figure 2a: the contribution (%) of CO emission from fires occurred inside the SENEX domain**

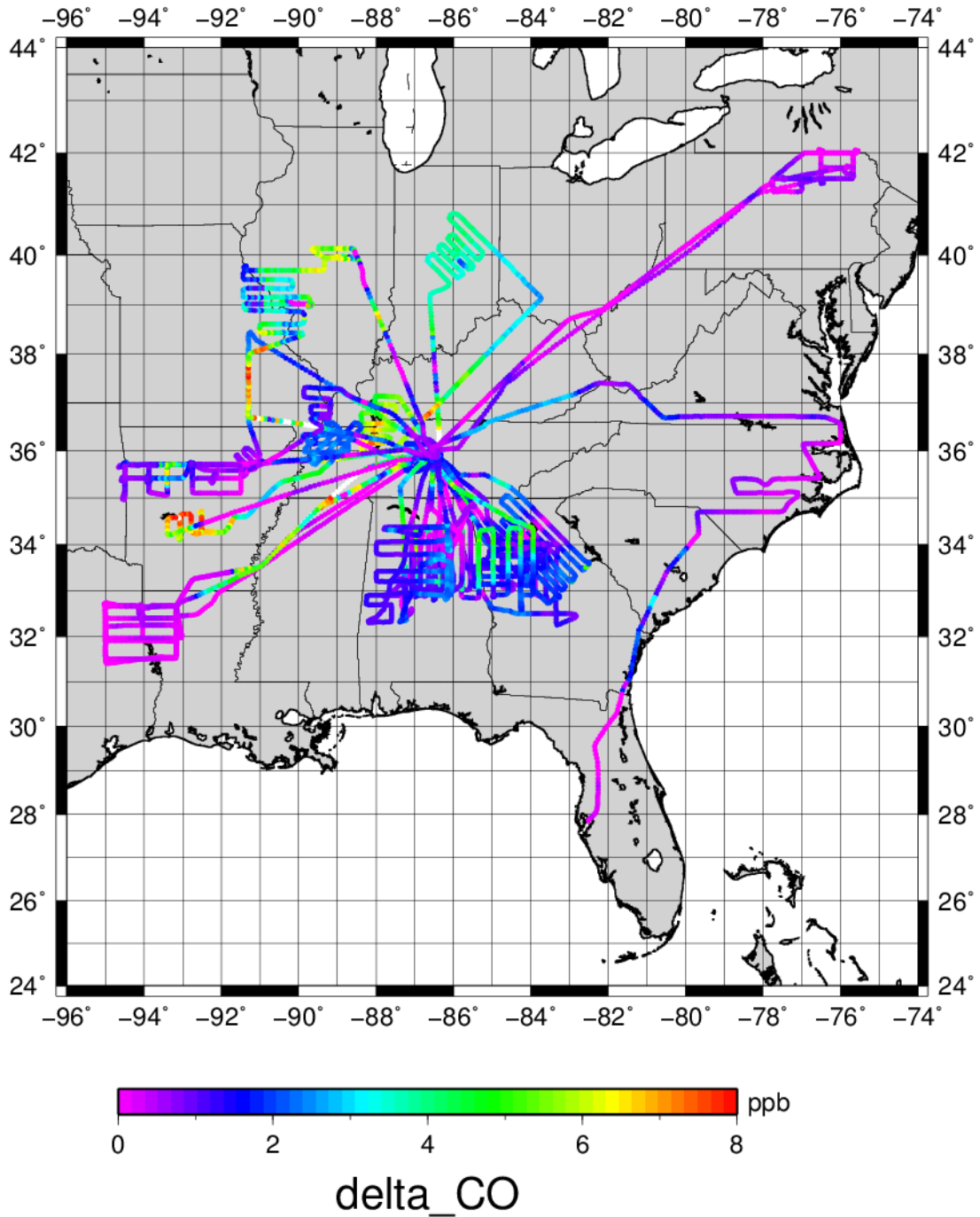


523

524 **Figure 2b: the contribution (%) of CO flux flowing into the SENEX domain from its boundary caused by**
525 **fires burning outside the SENEX domain but inside the CONUS domain**

526

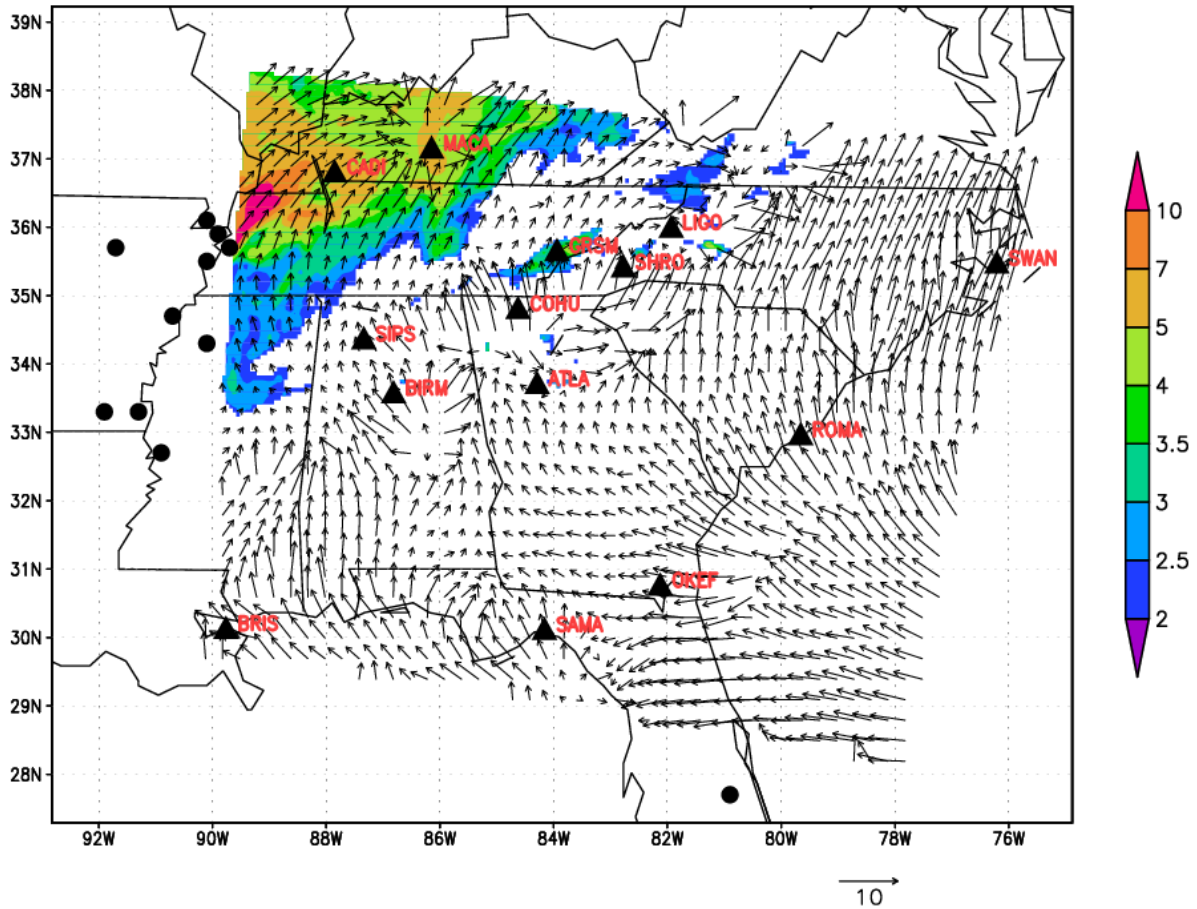
527



528

529 **Figure 3: Simulated ΔCO (ppb) extracted along a SENEX flight path (on which day? By which airplane?)**
 530 **The color bar depicts the difference in concentration between ?? and ??. The color shading along the**
 531 **transect corresponds to such concentration difference between the two realizations.**

532



533

534 **Figure 4: Simulated ΔCO (>2.0 ppb) in the SENEX domain on June 24 2013 overlaid with 2 m wind**
 535 **arrows with a 10 m s^{-1} reference arrow shown in the bottom right. (Is the wind daily averaged wind? If**
 536 **not the valid time needed to be given). The solid black circle is detected fire hotspots by HMS. The**
 537 **solid triangle labeled with station code represents IMPROVE sites used in model verification**
 538 **calculations.**

539

540

541

542

543

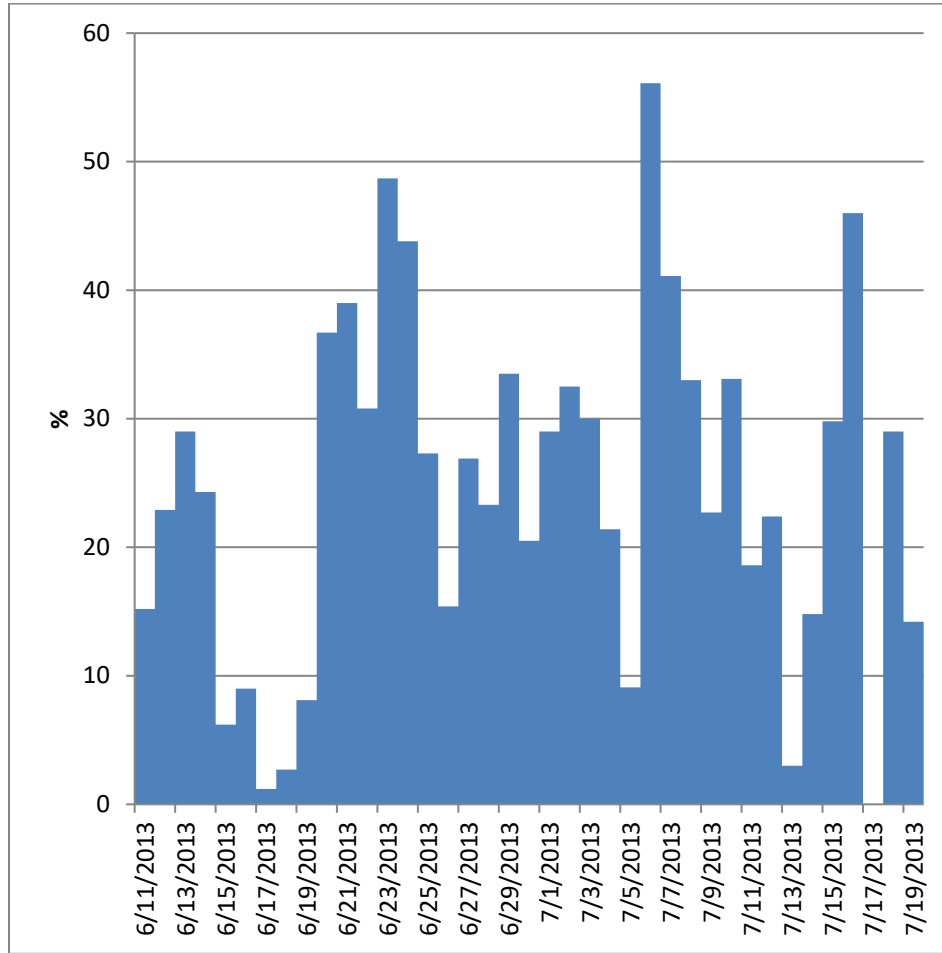
544

545

546

547

548



549

550

Figure 5: FMS (Figure of Merits in Space) (%) from June 11 to July 19 in 2013 during SENEX

551

552

553

554

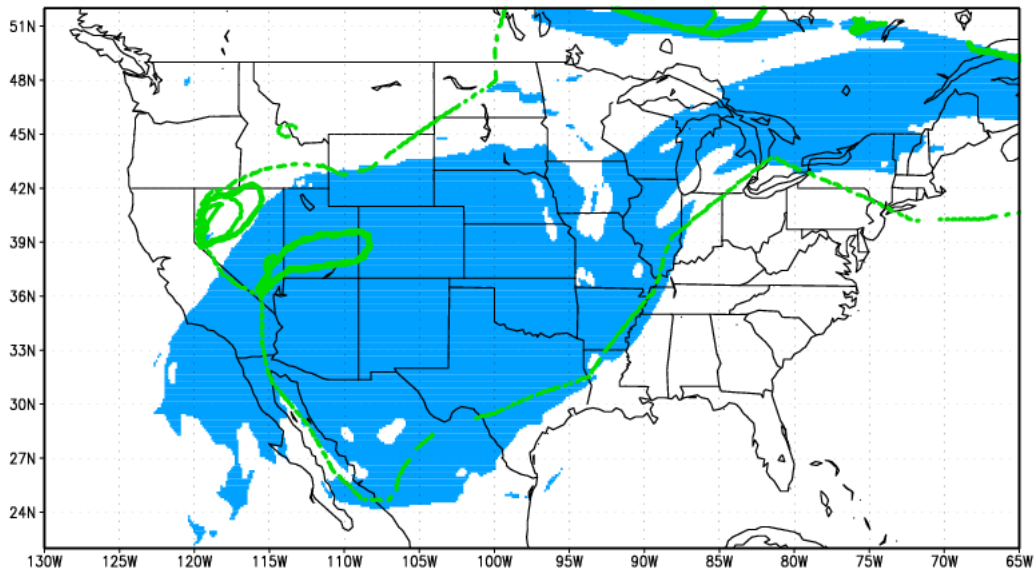
555

556

557

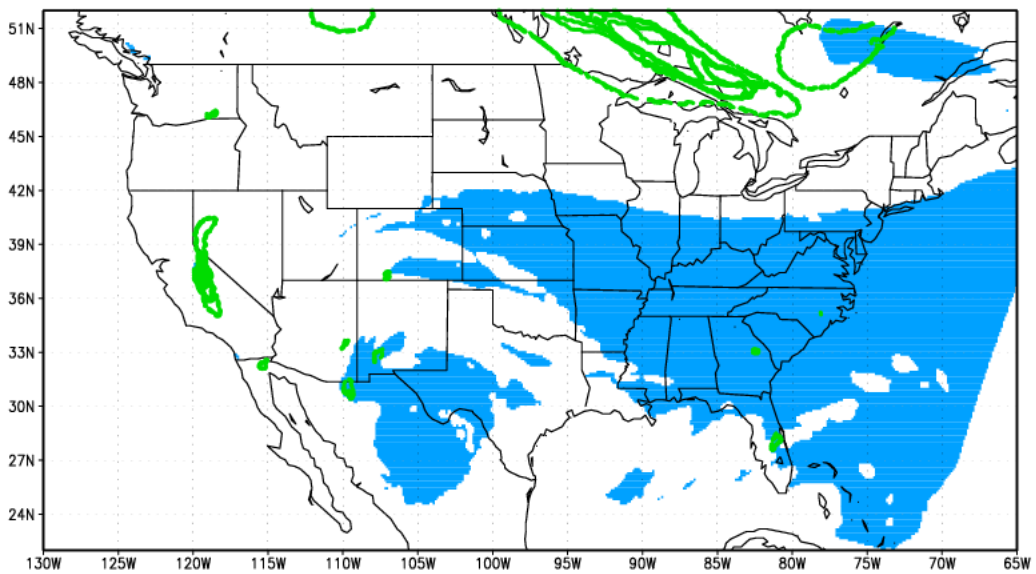
558

559



560

561 **Figure 6a: HMS observed plume shape versus CMAQ predicted plume shape on July 6 2013 (truly**
562 **averaged over 24 hours? If not, the averaging scheme needed to be stated here?); The light blue**
563 **shading represents modeled plume shape (defined as total column ΔCO) and the thin dash line and**
564 **emboldened green lines encircle areas representing HMS-derived light and strong influenced plume**
565 **shape, respectively.**

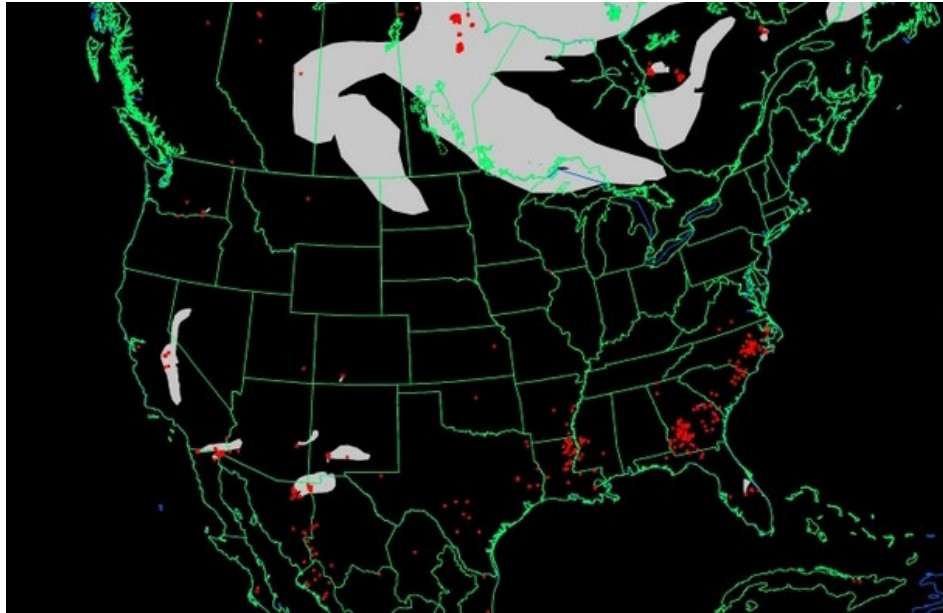


566

567

Figure 6b: Same as Figure 6a but for June 17 2013

568

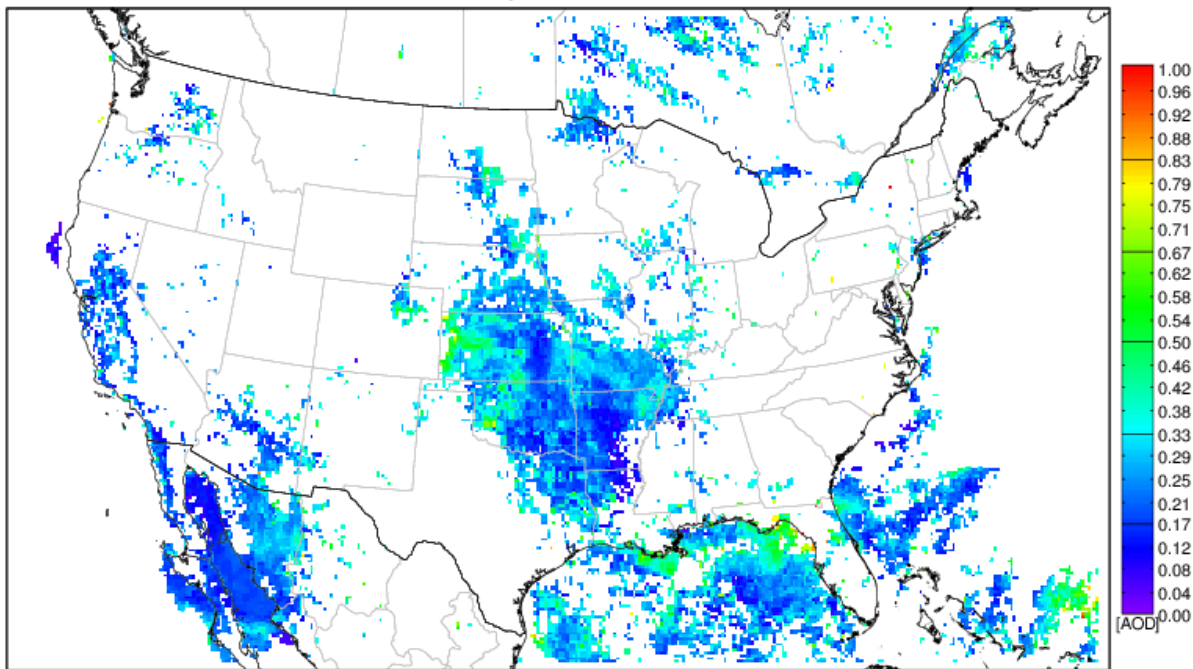


569

570 **Figure 6c: HMS detected fire hotspots (red) and smoke plume shapes (white) on June 17 2013**

571

(<http://ready.arl.noaa.gov/data/archives/fires/national/arcweb>)

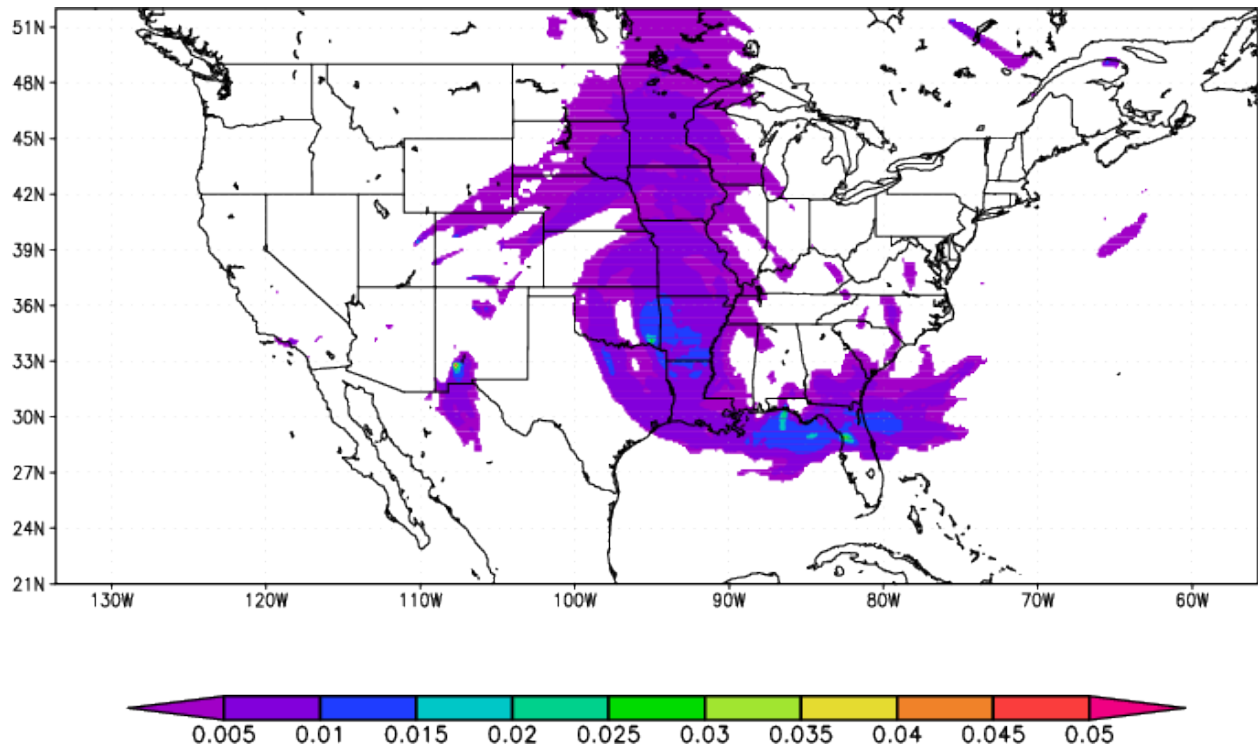


572

573 **Figure 7a: GOES detected AOD influenced by fires using ASDTA diagnose method on June 14 2013.**

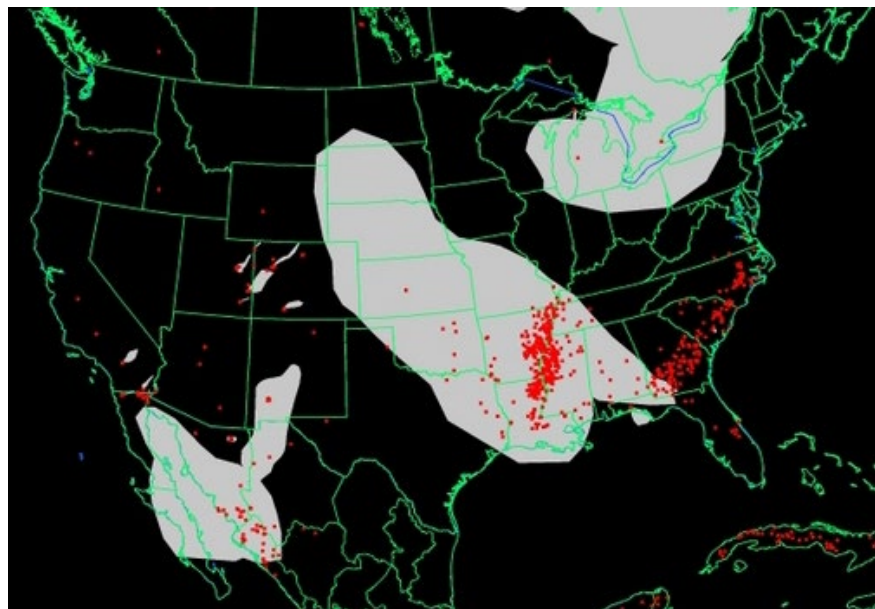
574 **Color-shaded region represents the fire-smoke influenced areas and the color denotes the magnitude**

575 **of the retrieved AOD.**



576

577 **Figure 7b: simulated Δ AOD (with-fire – without-fire) calculated in CMAQ on June 14 2013.**

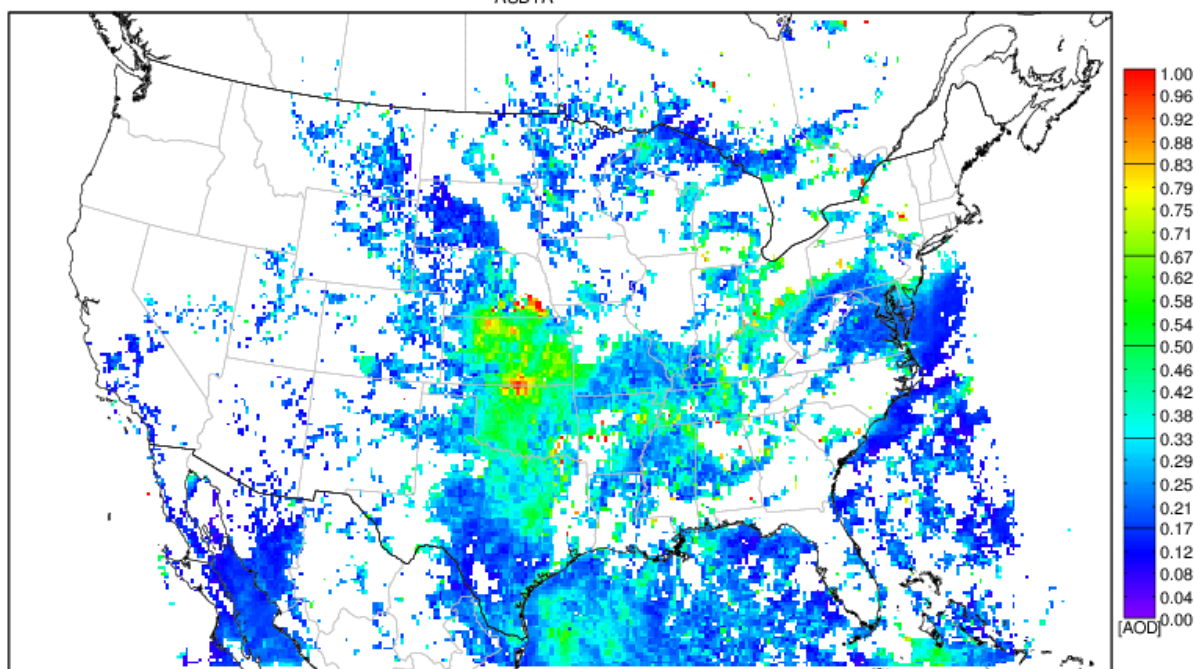


578

579 **Figure 7c: HMS detected fire hot spots (red) and smoke plume shapes (white) on June 14 2013**
580 **(<http://ready.arl.noaa.gov/data/archives/fires/national/arcweb>)**

581

582



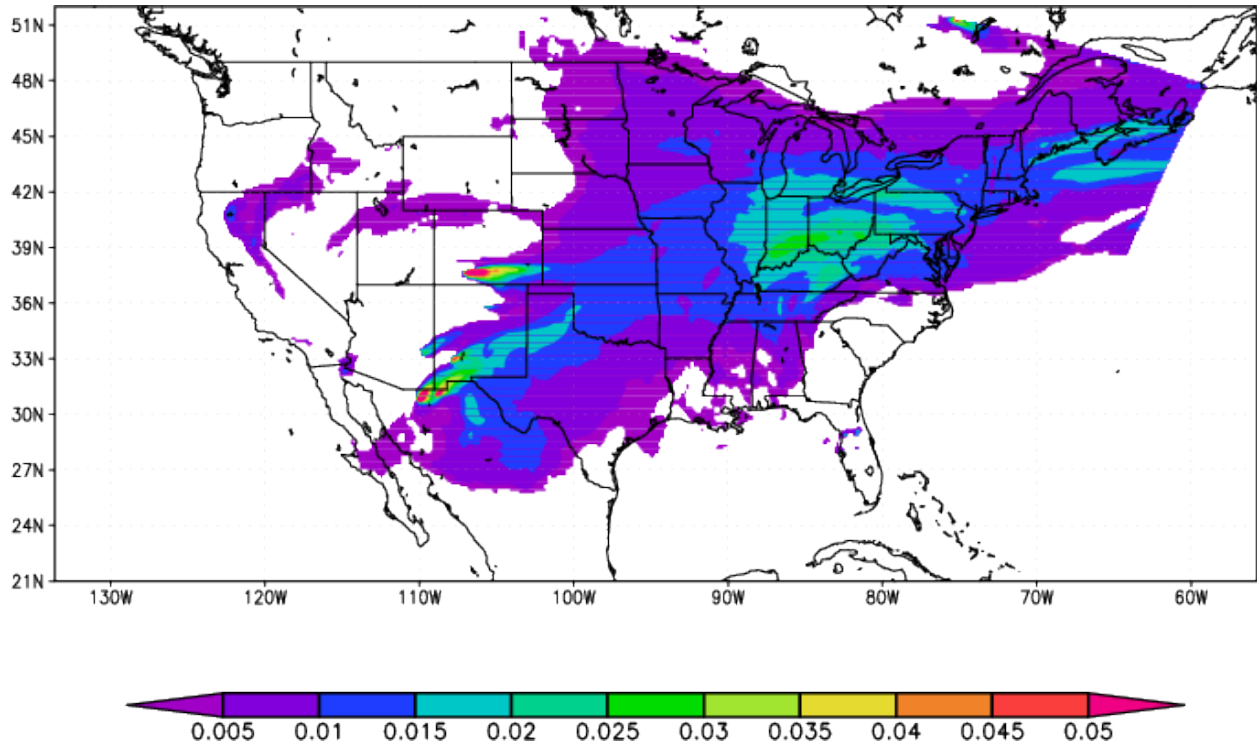
583

584 **Figure 7d: GOES detected AOD influenced by fires using ASDTA diagnose method on June 25 2013.**

585 **Color-shaded region represents the fire-smoke influenced areas and the color denotes the magnitude**

586 **of the retrieved AOD.**

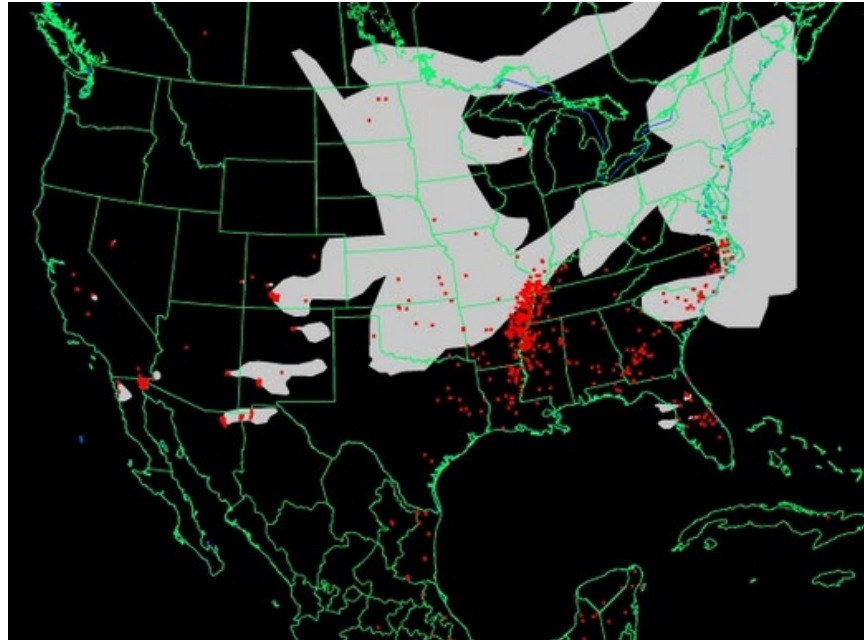
587



588

589

Figure 7e: simulated ΔAOD (withfire – nofire) calculated by CMAQ on June 25 2013.



590

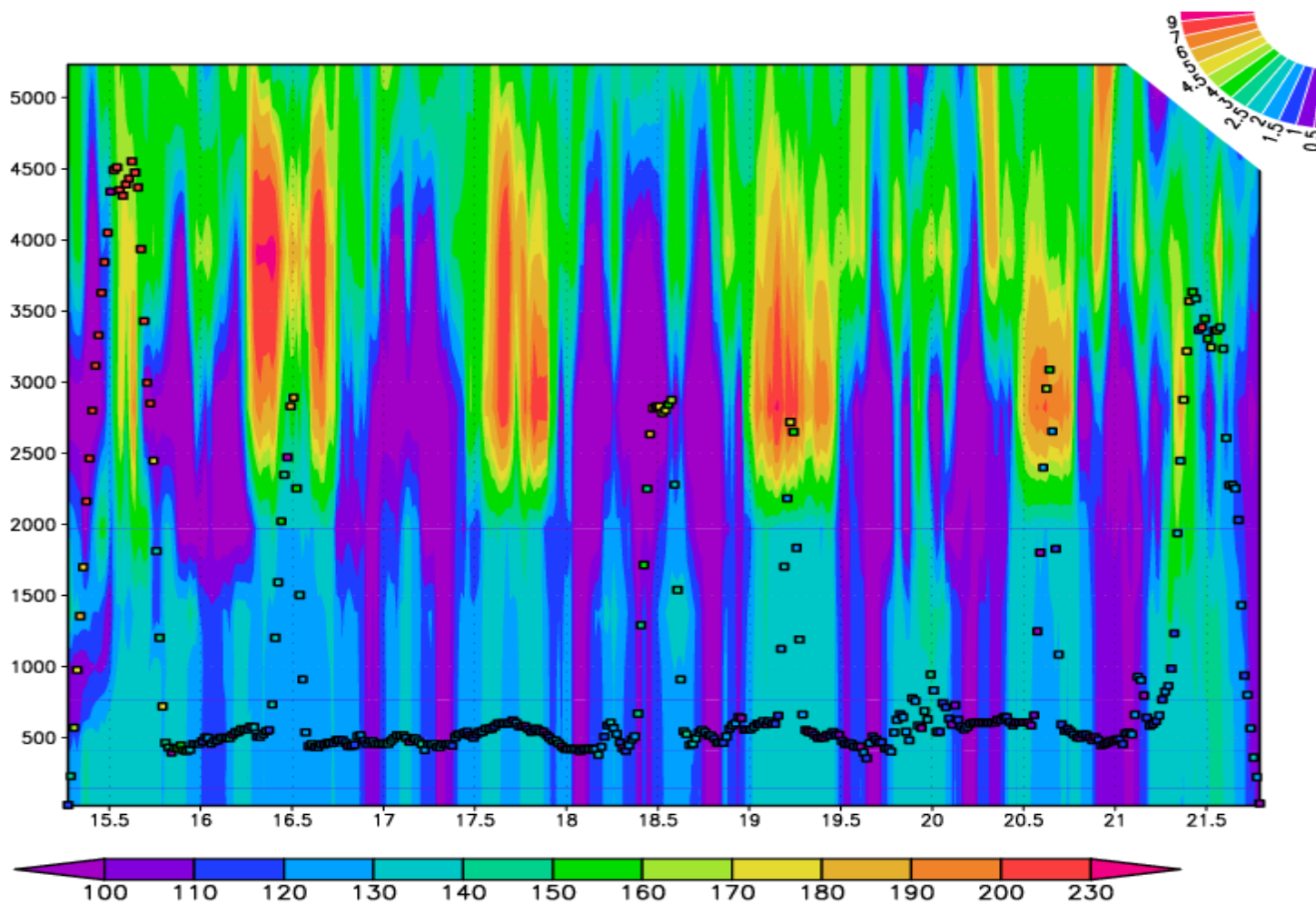
591

592

593

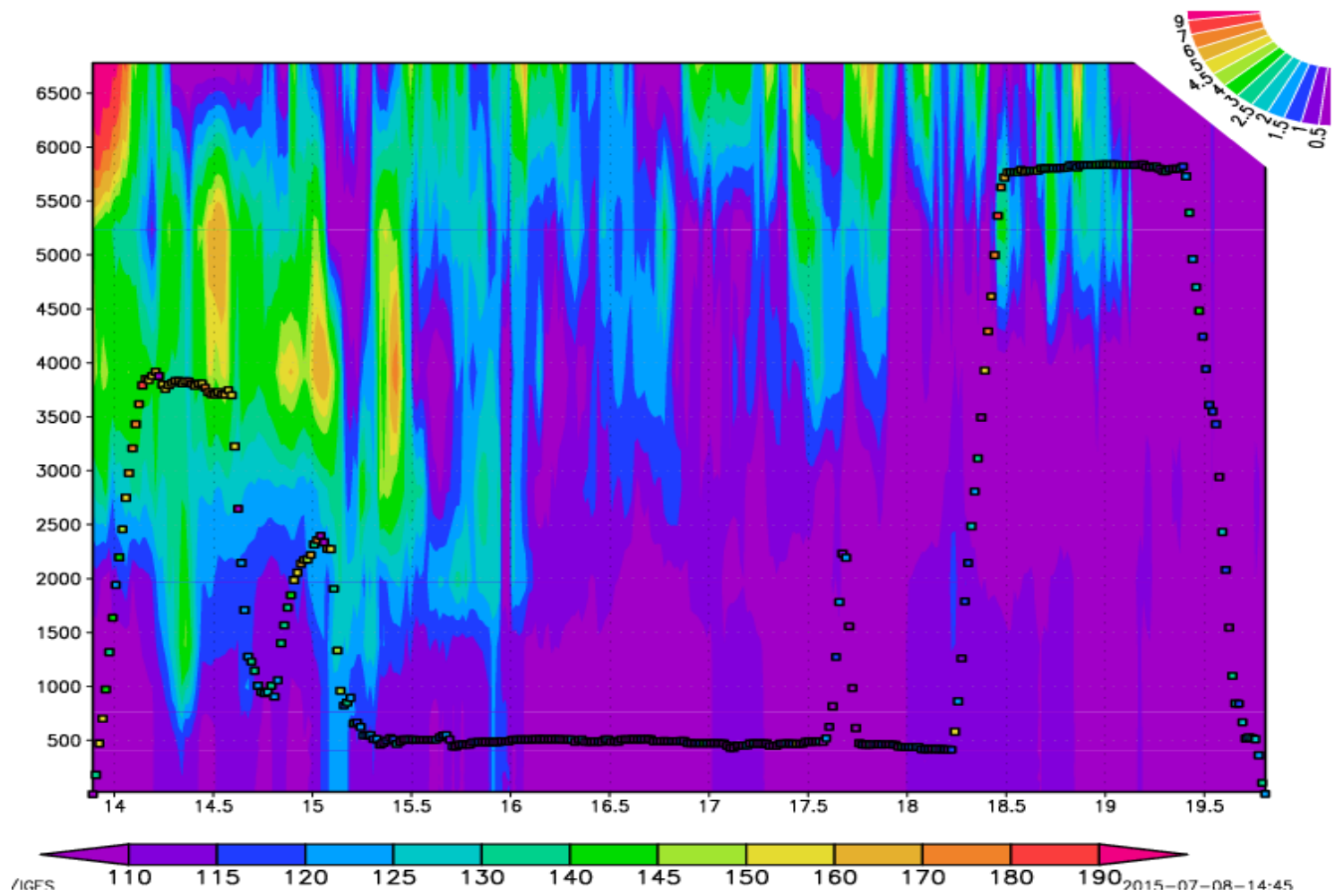
Figure 7f: HMS detected fire hot spots (red) and smoke plume shapes (white) on June 25 2013
<http://ready.arl.noaa.gov/data/archives/fires/national/arcweb>

594



595

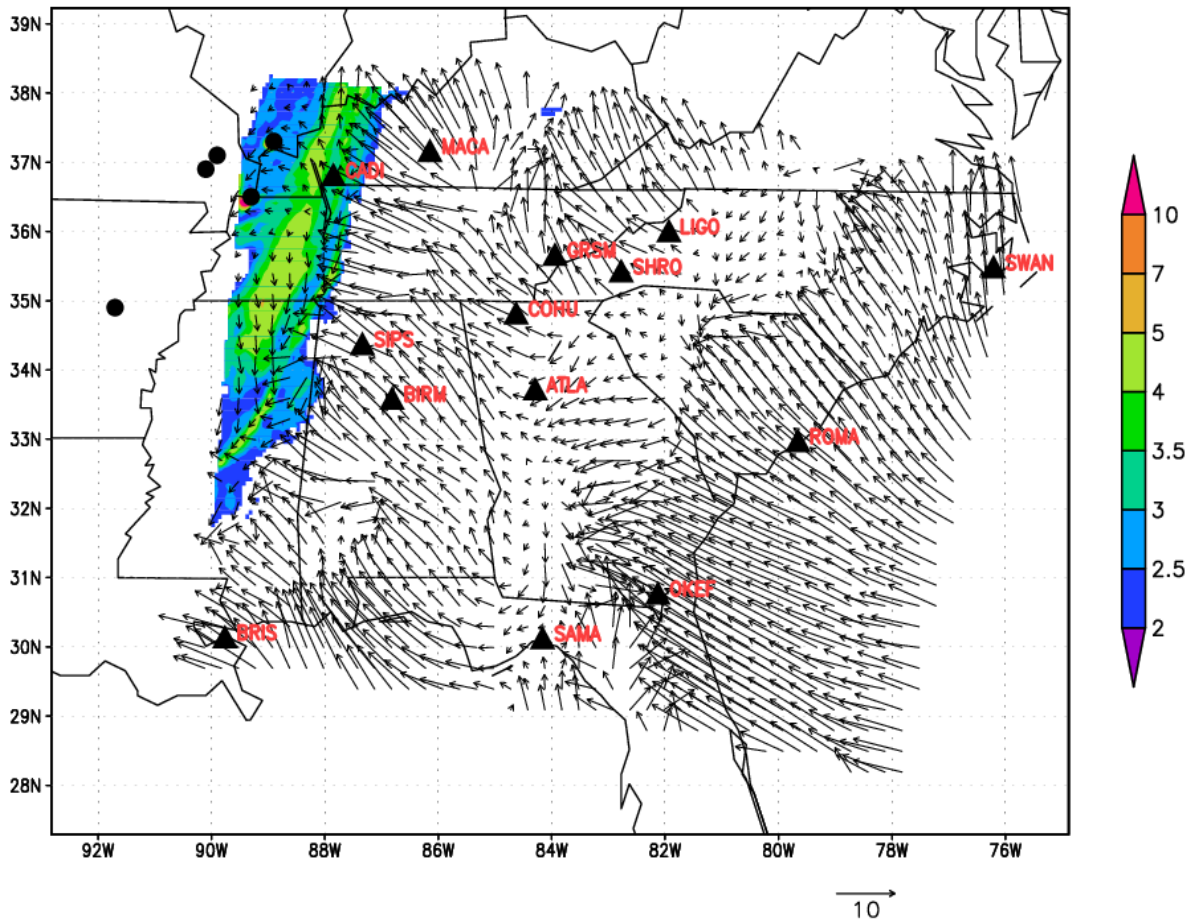
596 Figure 8a: Vertical distributions of CMAQ simulated ΔCO (ppb) shown along flight transect on June 16 2013. The x-axis label is UTC (hour) and
597 y-axis label is AGL (m). Two color bars represent observed CH_3CN concentration (open square dots and rectangle bar in ppt) and simulated
598 ΔCO concentration (backdrop color shading and fan bar in ppb), respectively.



599
600
601

Figure 8b: Same as Figure 8a but for July 10 2013.

602



603

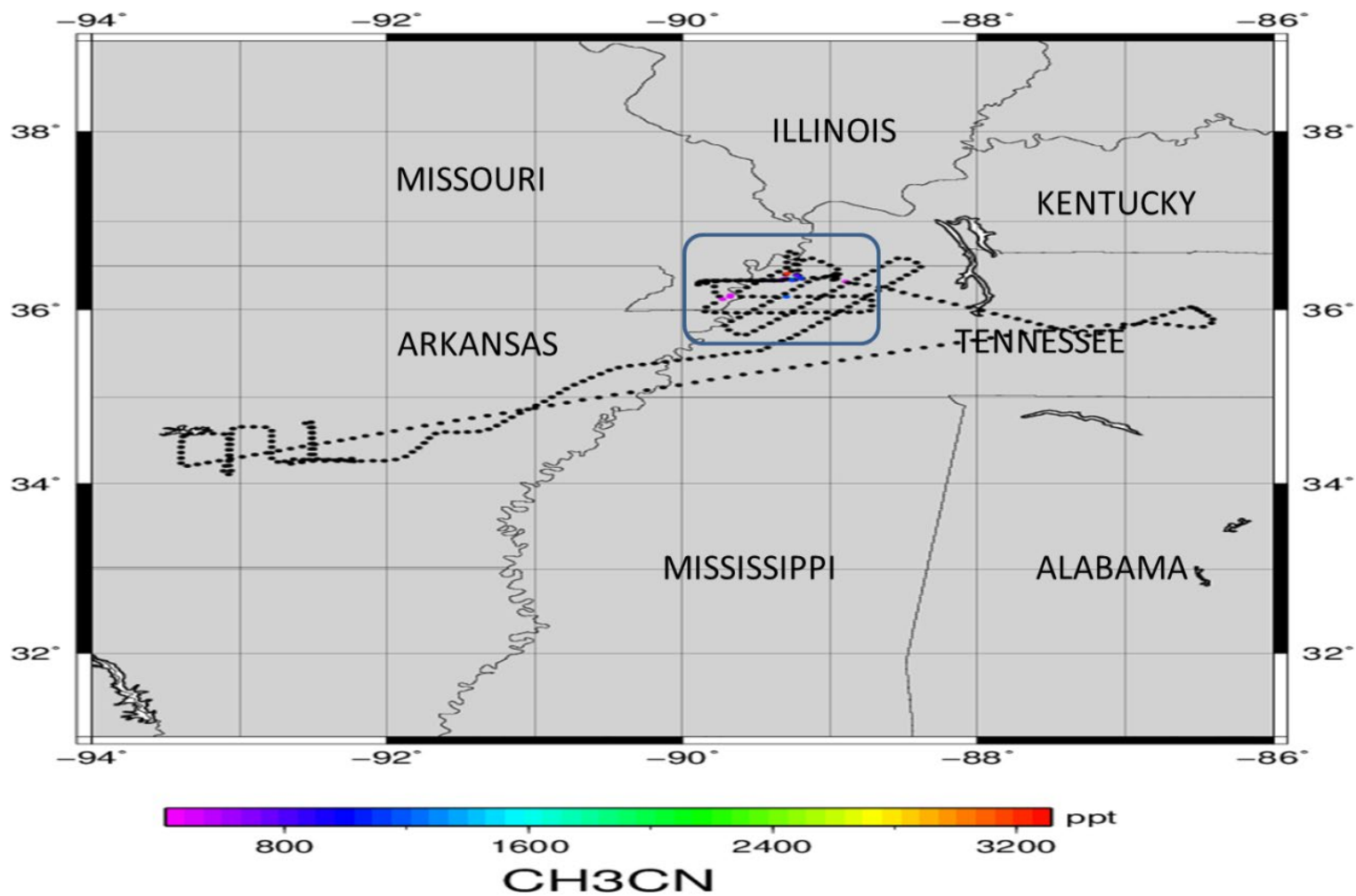
604

605

606

Figure 9a: Same as Figure 4 but for July 03 2013.

607



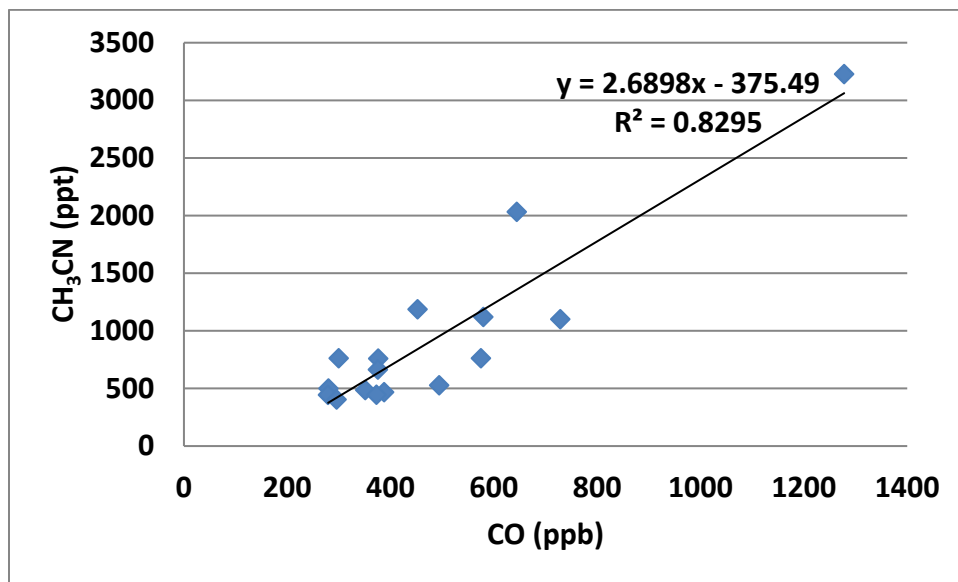
608

609

610

Figure 9b: the flight path of SENEX #0703 traversed the Central Plain between locale time ??? and ?? on ? 2013 --- colored by measured CH₃CN concentration (ppt)

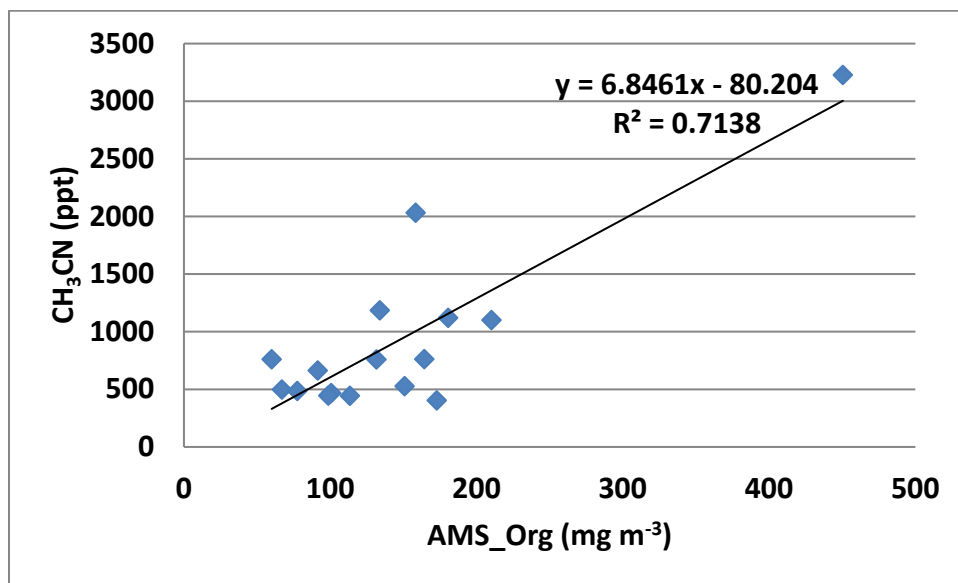
611



612

613

Figure 9c: CH₃CN (ppt) vs CO (ppb) scatter plot

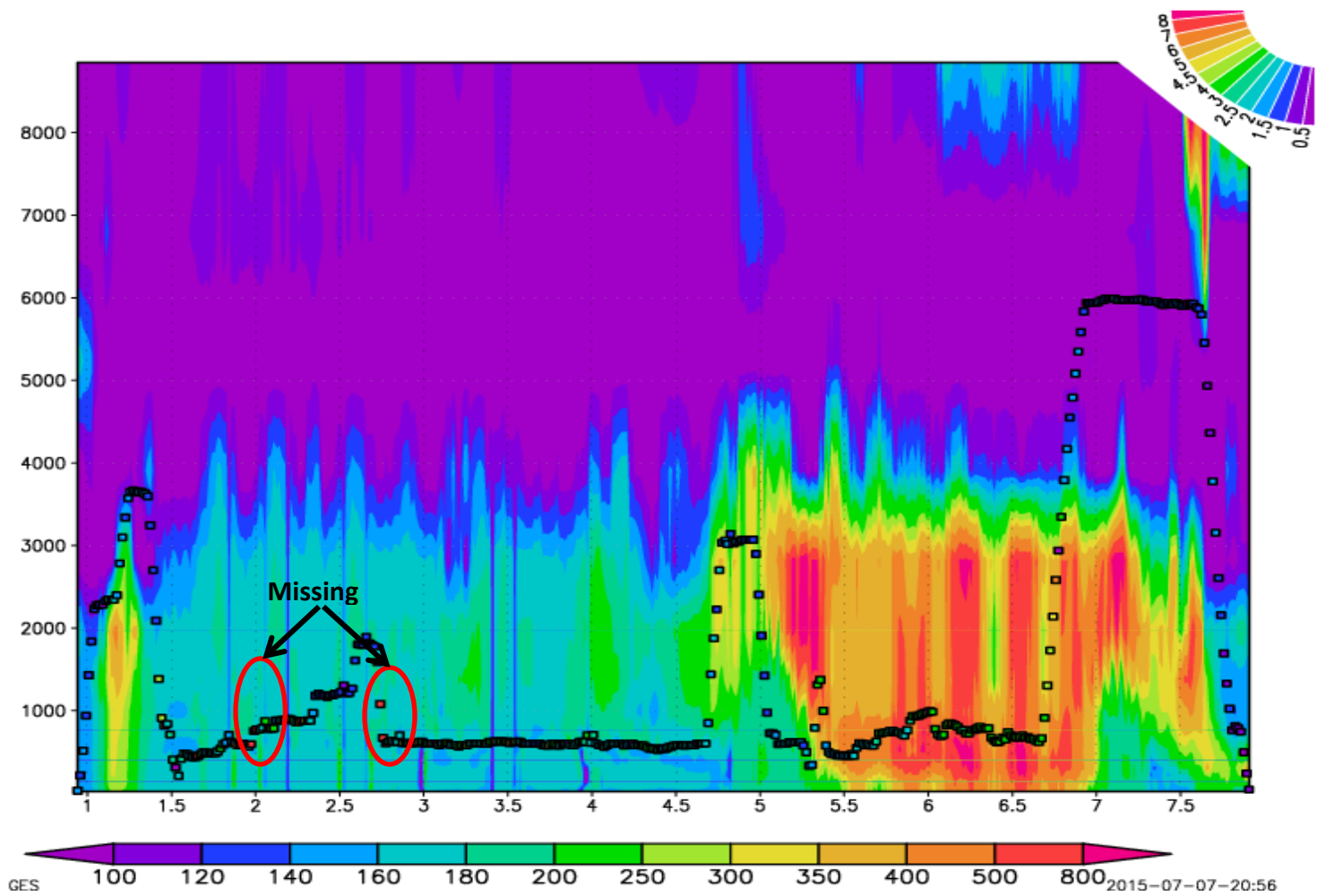


614

615

616

Figure 9d: CH₃CN (ppt) vs AMS_Org (mg m⁻³) scatter plot

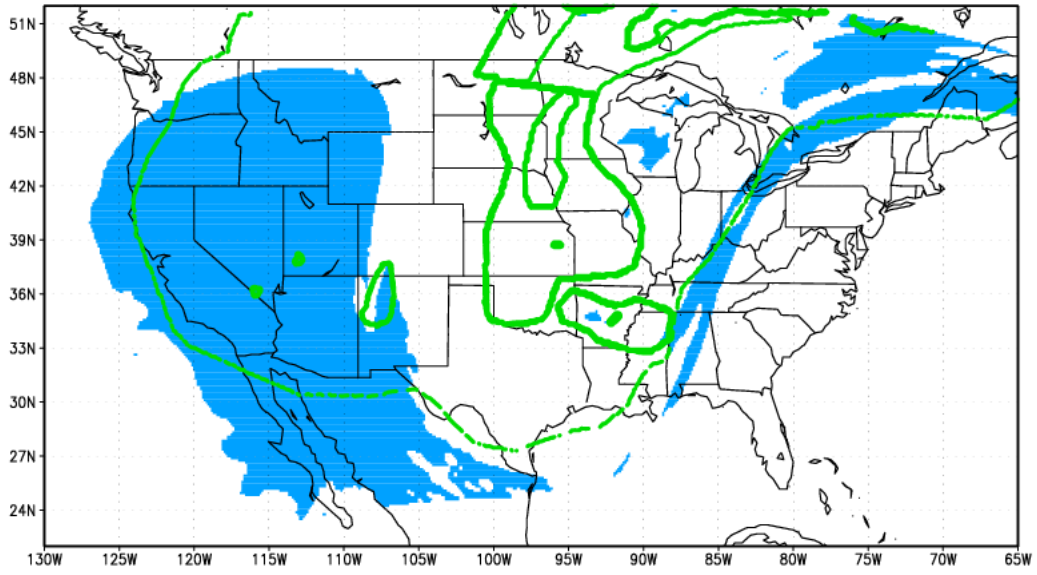


617

618

619

Figure 9e: Same as Figure 8a but for July 03 2013.



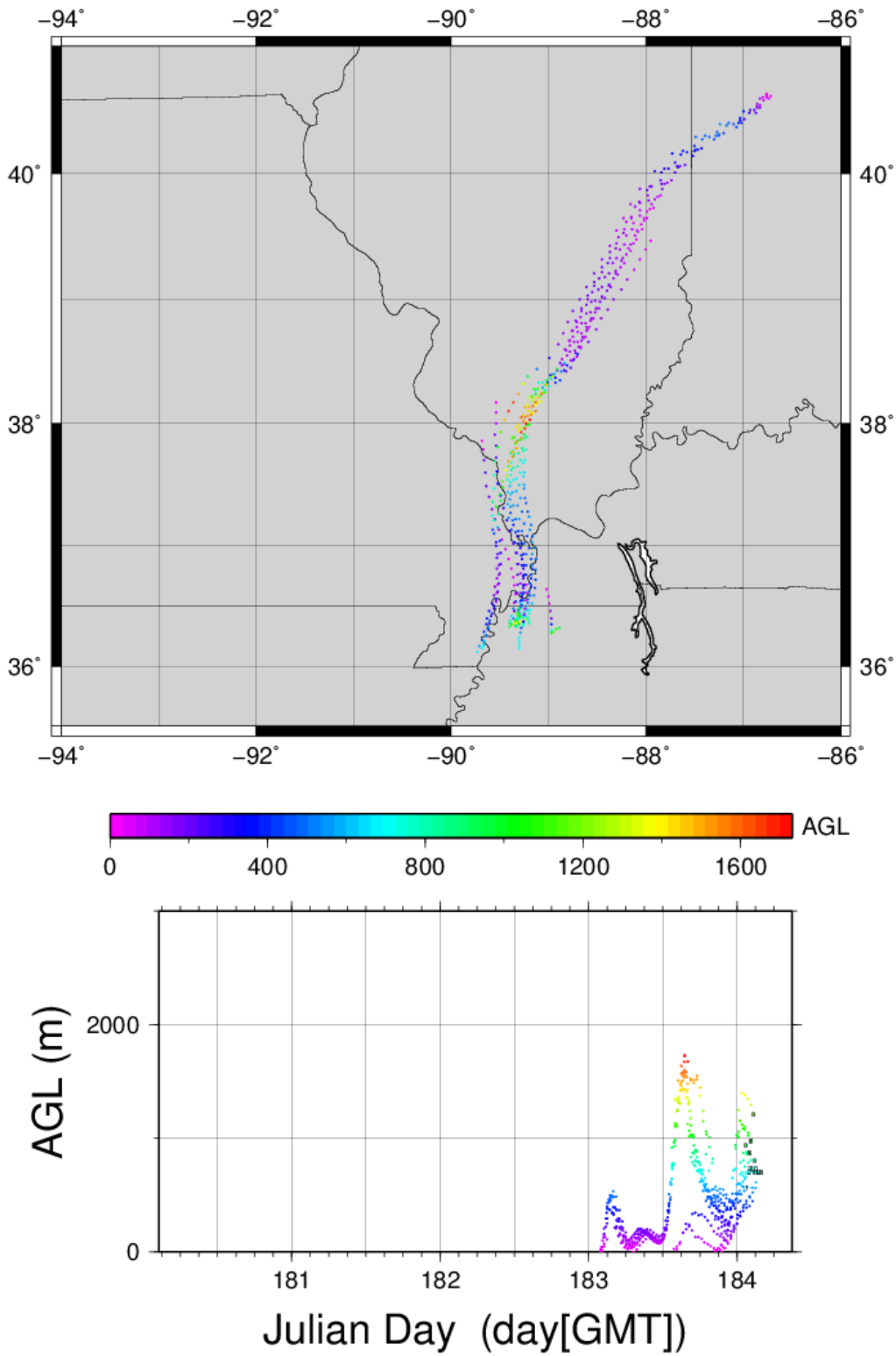
620

621

622

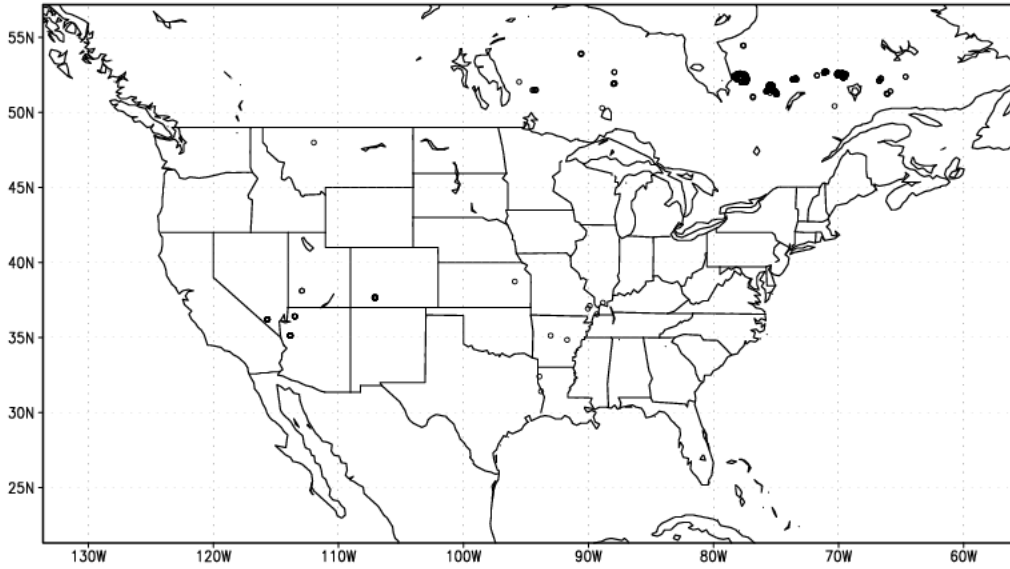
623

Figure 9f: Same as Figure 6a but for July 03 2013.



624

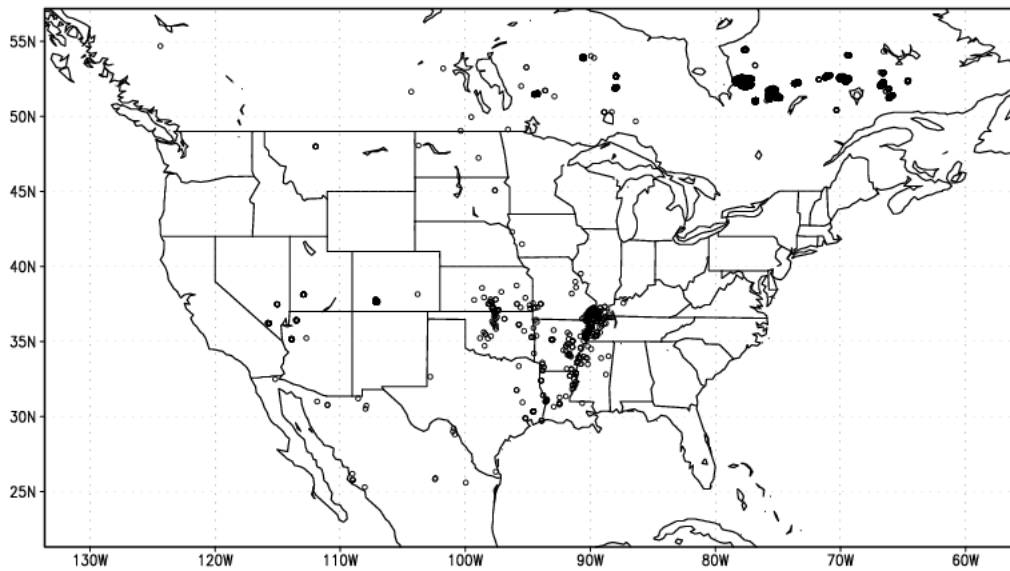
625 **Figure 10, a backward trajectory analysis for the observations obtained during the SENEX flight on July**
 626 **03 with CH₃CN measured concentration above 400 ppt.**



627

628

Figure 11a: fire hotspots in hmxhysplit.txt on July 03 2013



629

630

Figure 11b: fire hotspots in hmx.txt on July 03 2013

631

632

633

634

635

636 **Tables:**

637 **Table 1: observed and simulated CO (ppb) during NOAA SENEX**

AGL (m)	SAMPLE SIZE	OBS	OBS_MAX	Mod_withfire	Mod_nofire	ΔCO
<500	166	128.93±38.51	319.55	108.70±21.37	107.16±20.34	1.54
500~1000	3565	146.19±44.39	1277.97	108.39±19.82	106.50±18.86	1.88
1000~1500	793	125.41±28.09	299.64	100.11±15.63	98.49±14.67	1.62
1500~2000	306	119.68±23.99	265.29	100.75±17.04	99.08±15.89	1.67
2000~2500	219	111.48±19.98	286.22	99.88±17.95	98.37±16.92	1.51
2500~3000	209	111.84±19.79	295.79	97.43±12.21	95.87±11.15	1.56
3000~3500	181	109.31±16.66	197.94	89.34±12.09	88.13±11.06	1.21
3500~4000	195	110.78±14.36	140.42	92.11±10.73	90.25±9.62	1.86
4000~5000	369	89.82±19.09	138.04	80.36±10.15	79.17±9.14	1.19
5000~6000	354	102.26±22.37	209.20	78.12±7.64	76.82±6.28	1.30
6000~7000	85	87.53±17.88	115.32	73.35±4.71	70.58±2.45	2.77

638

639

640

641

642 **Table 2: identified fire signals from IMPROVE measurements during SENEX**

Site	Date	Concentrations (ug m ⁻³)						Ratio (Concentration/Average)						Ratio	
		EC	OC	K	SOIL	NO ₃ ⁻	SO ₄ ²⁻	EC	OC	K	SOIL	NO ₃ ⁻	SO ₄ ²⁻	BC/OC	K/BC
COHU	0621	0.28	2.10	0.05	0.22	0.13	2.61	1.4	1.46	1.42	0.39	0.84	1.28	0.1331	0.1933
MACA	0624	0.45	2.34	0.09	0.26	0.24	2.76	1.85	1.58	1.82	0.48	1.19	1.24	0.1929	0.1973
MACA	0703	0.33	2.32	0.08	0.16	0.29	2.11	1.35	1.57	1.73	0.29	1.43	0.94	0.1423	0.2554
BRIS	0703	0.24	0.98	0.21	0.31	0.11	2.63	1.49	1.28	2.79	0.13	0.35	1.36	0.2458	0.8851
GRSM	0621	0.25	1.56	0.05	0.24	0.13	2.52	1.36	1.45	1.24	0.49	0.99	1.42	0.1596	0.1979

643 Notes: (ratios for EC, OC and K > 1.2) **U** (ratio for SOIL < 1.0) **U** (ratios for NO₃⁻ and SO₄²⁻ < 1.5);

644

645

646

647

648

649

650

651 **References:**

- 652 Achtemeier, G. L., S. A. Goodrick, Y. Q. Liu, F. Garcia-Menendez, Y. T. Hu, and M. T. Odman. Modeling
653 Smoke Plume-Rise and Dispersion from Southern United States Prescribed Burns with
654 Daysmoke, *Atmosphere*, 2: 358-88. doi:10.3390/atmos2030358, 2011.
- 655 Aiken, A. C., B. de Foy, C. Wiedinmyer, P. F. DeCarlo, I. M. Ulbrich, M. N. Wehrli, S. Szidat, A. S. H. Prevot,
656 J. Noda, L. Wacker, R. Volkamer, E. Fortner, J. Wang, A. Laskin, V. Shutthanandan, J. Zheng, R.
657 Zhang, G. Paredes-Miranda, W. P. Arnott, L. T. Molina, G. Sosa, X. Querol, and J. L. Jimenez.
658 Mexico city aerosol analysis during MILAGRO using high resolution aerosol mass spectrometry at
659 the urban supersite (T0) - Part 2: Analysis of the biomass burning contribution and the non-fossil
660 carbon fraction, *Atmospheric Chemistry and Physics*, 10: 5315-41. doi:10.5194/acp-10-5315-
661 2010, 2010.
- 662 Alvarado, M. J., C. R. Lonsdale, R. J. Yokelson, S. K. Akagi, H. Coe, J. S. Craven, E. V. Fischer, G. R.
663 McMeeking, J. H. Seinfeld, T. Soni, J. W. Taylor, D. R. Weise, and C. E. Wold. Investigating the
664 links between ozone and organic aerosol chemistry in a biomass burning plume from a
665 prescribed fire in California chaparral, *Atmospheric Chemistry and Physics*, 15: 6667-88.
666 doi:10.5194/acp-15-6667-2015, 2015.
- 667 Baker, K. R., M. C. Woody, G. S. Tonnesen, W. Hutzell, H. O. T. Pye, M. R. Beaver, G. Pouliot, and T.
668 Pierce. Contribution of regional-scale fire events to ozone and PM2.5 air quality estimated by
669 photochemical modeling approaches, *Atmospheric Environment*, 140: 539-54.
670 doi:10.1016/j.atmosenv.2016.06.032, 2016.
- 671 Carlton, A. G., P. V. Bhave, S. L. Napelenok, E. D. Edney, G. Sarwar, R. W. Pinder, G. A. Pouliot, and M.
672 Houyoux. Model Representation of Secondary Organic Aerosol in CMAQv4.7, *Environmental*
673 *Science & Technology*, 44: 8553-60. doi:10.1021/es100636q, 2010.
- 674 Chai, T., H. C. Kim, P. Lee, D. Tong, L. Pan, Y. Tang, J. Huang, J. McQueen, M. Tsidulko, and I. Stajner.
675 Evaluation of the United States National Air Quality Forecast Capability experimental real-time
676 predictions in 2010 using Air Quality System ozone and NO2 measurements, *Geoscientific Model*
677 *Development*, 6: 1831-50. doi:10.5194/gmd-6-1831-2013, 2013.
- 678 Davis, A. Y., R. Ottmar, Y. Q. Liu, S. Goodrick, G. Achtemeier, B. Gullett, J. Aurell, W. Stevens, R.
679 Greenwald, Y. T. Hu, A. Russell, J. K. Hiers, and M. T. Odman. Fire emission uncertainties and
680 their effect on smoke dispersion predictions: a case study at Eglin Air Force Base, Florida, USA,
681 *International Journal of Wildland Fire*, 24: 276-85. doi:10.1071/wf13071, 2015.
- 682 de Gouw, J. A., C. Warneke, D. D. Parrish, J. S. Holloway, M. Trainer, and F. C. Fehsenfeld. Emission
683 sources and ocean uptake of acetonitrile (CH3CN) in the atmosphere, *Journal of Geophysical*
684 *Research-Atmospheres*, 108. doi:10.1029/2002jd002897, 2003.
- 685 DeBell, L. J., R. W. Talbot, J. E. Dibb, J. W. Munger, E. V. Fischer, and S. E. Frolking. A major regional air
686 pollution event in the northeastern United States caused by extensive forest fires in Quebec,
687 Canada, *Journal of Geophysical Research-Atmospheres*, 109. doi:10.1029/2004jd004840, 2004.
- 688 Delfino, R. J., S. Brummel, J. Wu, H. Stern, B. Ostro, M. Lipsett, A. Winer, D. H. Street, L. Zhang, T. Tjoa,
689 and D. L. Gillen. The relationship of respiratory and cardiovascular hospital admissions to the
690 southern California wildfires of 2003, *Occupational and Environmental Medicine*, 66: 189-97.
691 doi:10.1136/oem.2008.041376, 2009.
- 692 Draxler, R. R., and G. D. Hess. An overview of the HYSPLIT_4 modelling system for trajectories, dispersion
693 and deposition, *Australian Meteorological Magazine*, 47: 295-308. 1998.
- 694 Dreessen, J., J. Sullivan, and R. Delgado. Observations and impacts of transported Canadian wildfire
695 smoke on ozone and aerosol air quality in the Maryland region on June 9-12, 2015, *Journal of*
696 *the Air & Waste Management Association*, 66: 842-62. doi:10.1080/10962247.2016.1161674,
697 2016.

698 Drury, S. A., N. Larkin, T. T. Strand, S. M. Huang, S. J. Strenfel, E. M. Banwell, T. E. O'Brien, and S. M.
699 Raffuse. INTERCOMPARISON OF FIRE SIZE, FUEL LOADING, FUEL CONSUMPTION, AND SMOKE
700 EMISSIONS ESTIMATES ON THE 2006 TRIPOD FIRE, WASHINGTON, USA, *Fire Ecology*, 10: 56-83.
701 doi:10.4996/fireecology.1001056, 2014.

702 Eatough, D. J., D. A. Eatough, L. Lewis, and E. A. Lewis. Fine particulate chemical composition and light
703 extinction at Canyonlands National Park using organic particulate material concentrations
704 obtained with a multisystem, multichannel diffusion denuder sampler, *Journal of Geophysical
705 Research-Atmospheres*, 101: 19515-31. doi:10.1029/95jd01385, 1996.

706 Erbrink, H. J. PLUME RISE IN DIFFERENT ATMOSPHERES - A PRACTICAL SCHEME AND SOME
707 COMPARISONS WITH LIDAR MEASUREMENTS, *Atmospheric Environment*, 28: 3625-36.
708 doi:10.1016/1352-2310(94)00197-s, 1994.

709 Giglio, L., J. Descloitres, C. O. Justice, and Y. J. Kaufman. An enhanced contextual fire detection algorithm
710 for MODIS, *Remote Sensing of Environment*, 87: 273-82. doi:10.1016/s0034-4257(03)00184-6,
711 2003.

712 Hamm, S., and P. Warneck. THE INTERHEMISPHERIC DISTRIBUTION AND THE BUDGET OF ACETONITRILE
713 IN THE TROPOSPHERE, *Journal of Geophysical Research-Atmospheres*, 95: 20593-606.
714 doi:10.1029/JD095iD12p20593, 1990.

715 Hardy, C. C., and C. E. Hardy. Fire danger rating in the United States of America: an evolution since 1916,
716 *International Journal of Wildland Fire*, 16: 217-31. doi:10.1071/wf06076, 2007.

717 Herron-Thorpe, F. L., G. H. Mount, L. K. Emmons, B. K. Lamb, D. A. Jaffe, N. L. Wigder, S. H. Chung, R.
718 Zhang, M. D. Woelfle, and J. K. Vaughan. Air quality simulations of wildfires in the Pacific
719 Northwest evaluated with surface and satellite observations during the summers of 2007 and
720 2008, *Atmospheric Chemistry and Physics*, 14: 12533-51. doi:10.5194/acp-14-12533-2014, 2014.

721 Holzinger, R., C. Warneke, A. Hansel, A. Jordan, W. Lindinger, D. H. Scharffe, G. Schade, and P. J. Crutzen.
722 Biomass burning as a source of formaldehyde, acetaldehyde, methanol, acetone, acetonitrile,
723 and hydrogen cyanide, *Geophysical Research Letters*, 26: 1161-64. doi:10.1029/1999gl900156,
724 1999.

725 Hu, X. F., C. Yu, D. Tian, M. Ruminski, K. Robertson, L. A. Waller, and Y. Liu. Comparison of the Hazard
726 Mapping System (HMS) fire product to ground-based fire records in Georgia, USA, *Journal of
727 Geophysical Research-Atmospheres*, 121: 2901-10. doi:10.1002/2015jd024448, 2016.

728 Huang, J., J. McQueen, J. Wilczak, I. Djalalova, I. Stajner, P. Shafran, D. Allured, P. Lee, L. Pan, D. Tong, H.
729 Huang, G. DiMego, S. Upadhyay, and L. Monache. Improving NOAA NAQFC PM2.5 predictions
730 with a bias correction approach, *Wea. Forecasting*. doi:10.1175/WAF-D-16-0118.1, 2017.

731 Jaffe, D. A., N. Wigder, N. Downey, G. Pfister, A. Boynard, and S. B. Reid. Impact of Wildfires on Ozone
732 Exceptional Events in the Western US, *Environmental Science & Technology*, 47: 11065-72.
733 doi:10.1021/es402164f, 2013.

734 Johnston, F. H., S. B. Henderson, Y. Chen, J. T. Randerson, M. Marlier, R. S. DeFries, P. Kinney, Dmjs
735 Bowman, and M. Brauer. Estimated Global Mortality Attributable to Smoke from Landscape
736 Fires, *Environmental Health Perspectives*, 120: 695-701. doi:10.1289/ehp.1104422, 2012.

737 Justice, C. O., L. Giglio, S. Korontzi, J. Owens, J. T. Morisette, D. Roy, J. Descloitres, S. Alleaume, F.
738 Petitcolin, and Y. Kaufman. The MODIS fire products, *Remote Sensing of Environment*, 83: 244-
739 62. doi:10.1016/s0034-4257(02)00076-7, 2002.

740 Knorr, W., V. Lehsten, and A. Arneth. Determinants and predictability of global wildfire emissions,
741 *Atmospheric Chemistry and Physics*, 12: 6845-61. doi:10.5194/acp-12-6845-2012, 2012.

742 Larkin, N. K., S. M. O'Neill, R. Solomon, S. Raffuse, T. Strand, D. C. Sullivan, C. Krull, M. Rorig, J. L.
743 Peterson, and S. A. Ferguson. The BlueSky smoke modeling framework, *International Journal of
744 Wildland Fire*, 18: 906-20. doi:10.1071/wf07086, 2009.

745 Lee, Pius, Jeffery McQueen, Ivanka Stajner, Jianping Huang, Li Pan, Daniel Tong, Hyuncheol Kim, Youhua
746 Tang, Shobha Kondragunta, and Mark Ruminski. NAQFC developmental forecast guidance for
747 fine particulate matter (PM_{2.5}), *Weather and Forecasting*, 32: 343-60. doi:10.1175/waf-d-15-
748 0163.1, 2017.

749 Li, Z., S. Nadon, and J. Cihlar. Satellite-based detection of Canadian boreal forest fires: development and
750 application of the algorithm, *International Journal of Remote Sensing*, 21: 3057-69.
751 doi:10.1080/01431160050144956, 2000.

752 Malm, W. C., B. A. Schichtel, M. L. Pitchford, L. L. Ashbaugh, and R. A. Eldred. Spatial and monthly trends
753 in speciated fine particle concentration in the United States, *Journal of Geophysical Research-
754 Atmospheres*, 109. doi:10.1029/2003jd003739, 2004.

755 Neuman, J. A., M. Trainer, S. S. Brown, K. E. Min, J. B. Nowak, D. D. Parrish, J. Peischl, I. B. Pollack, J. M.
756 Roberts, T. B. Ryerson, and P. R. Veres. HONO emission and production determined from
757 airborne measurements over the Southeast US, *Journal of Geophysical Research-Atmospheres*,
758 121: 9237-50. doi:10.1002/2016jd025197, 2016.

759 Pan, L., D. Tong, P. Lee, H. C. Kim, and T. F. Chai. Assessment of NO_x and O₃ forecasting performances
760 in the US National Air Quality Forecasting Capability before and after the 2012 major emissions
761 updates, *Atmospheric Environment*, 95: 610-19. doi:10.1016/j.atmosenv.2014.06.020, 2014.

762 Pavlovic, R., J. Chen, K. Anderson, M. D. Moran, P. A. Beaulieu, D. Davignon, and S. Cousineau. The
763 FireWork air quality forecast system with near-real-time biomass burning emissions: Recent
764 developments and evaluation of performance for the 2015 North American wildfire season,
765 *Journal of the Air & Waste Management Association*, 66: 819-41.
766 doi:10.1080/10962247.2016.1158214, 2016.

767 Prados, A. I., S. Kondragunta, P. Ciren, and K. R. Knapp. GOES Aerosol/Smoke product (GASP) over North
768 America: Comparisons to AERONET and MODIS observations, *Journal of Geophysical Research-
769 Atmospheres*, 112. doi:10.1029/2006jd007968, 2007.

770 Prins, E. M., and W. P. Menzel. GEOSTATIONARY SATELLITE DETECTION OF BIOMASS BURNING IN
771 SOUTH-AMERICA, *International Journal of Remote Sensing*, 13: 2783-99. 1992.

772 Rappold, A. G., S. L. Stone, W. E. Cascio, L. M. Neas, V. J. Kilaru, M. S. Carraway, J. J. Szykman, A. Ising, W.
773 E. Cleve, J. T. Meredith, H. Vaughan-Batten, L. Deyneka, and R. B. Devlin. Peat Bog Wildfire
774 Smoke Exposure in Rural North Carolina Is Associated with Cardiopulmonary Emergency
775 Department Visits Assessed through Syndromic Surveillance, *Environmental Health Perspectives*,
776 119: 1415-20. doi:10.1289/ehp.1003206, 2011.

777 Reid, J. S., R. Koppmann, T. F. Eck, and D. P. Eleuterio. A review of biomass burning emissions part II:
778 intensive physical properties of biomass burning particles, *Atmospheric Chemistry and Physics*,
779 5: 799-825. 2005.

780 Rolph, G. D., R. R. Draxler, A. F. Stein, A. Taylor, M. G. Ruminski, S. Kondragunta, J. Zeng, H. C. Huang, G.
781 Manikin, J. T. McQueen, and P. M. Davidson. Description and Verification of the NOAA Smoke
782 Forecasting System: The 2007 Fire Season, *Weather and Forecasting*, 24: 361-78.
783 doi:10.1175/2008waf2222165.1, 2009.

784 Ruminski, M., and S. Kondragunta. Monitoring fire and smoke emissions with the hazard mapping
785 system - art. no. 64120B. in F. Kogan, S. Habib, V. S. Hegde and M. Matsuoka (eds.), *Disaster
786 Forewarning Diagnostic Methods and Management*. 2006.

787 Ruminski, M., J. Simko, J. Kibler, S. Kondragunta, R. Draxler, P. Davidson, and P. Li. Use of multiple
788 satellite sensors in NOAA's operational near real-time fire and smoke detection and
789 characterization program. in W. M. Hao (ed.), *Remote Sensing of Fire: Science and Application*.
790 2008.

791 Saide, P. E., D. A. Peterson, A. da Silva, B. Anderson, L. D. Ziemba, G. Diskin, G. Sachse, J. Hair, C. Butler,
792 M. Fenn, J. L. Jimenez, P. Campuzano-Jost, A. E. Perring, J. P. Schwarz, M. Z. Markovic, P. Russell,

793 J. Redemann, Y. Shinozuka, D. G. Streets, F. Yan, J. Dibb, R. Yokelson, O. B. Toon, E. Hyer, and G.
794 R. Carmichael. Revealing important nocturnal and day-to-day variations in fire smoke emissions
795 through a multiplatform inversion, *Geophysical Research Letters*, 42: 3609-18.
796 doi:10.1002/2015gl063737, 2015.

797 Sandberg, D.V., and J. Peterson. A source strength model for prescribed fires in coniferous logging slash,
798 *1984 annual meeting, Air Pollution Control Association, Northwest Section*. 14p. 1984.

799 Sapkota, A., J. M. Symons, J. Kleissl, L. Wang, M. B. Parlange, J. Ondov, P. N. Breyse, G. B. Diette, P. A.
800 Eggleston, and T. J. Buckley. Impact of the 2002 Canadian forest fires on particulate matter air
801 quality in Baltimore City, *Environmental Science & Technology*, 39: 24-32.
802 doi:10.1021/es035311z, 2005.

803 Schroeder, W., M. Ruminski, I. Csiszar, L. Giglio, E. Prins, C. Schmidt, and J. Morissette. Validation analyses
804 of an operational fire monitoring product: The Hazard Mapping System, *International Journal of*
805 *Remote Sensing*, 29: 6059-66. doi:10.1080/01431160802235845, 2008.

806 Singh, H. B., C. Cai, A. Kaduwela, A. Weinheimer, and A. Wisthaler. Interactions of fire emissions and
807 urban pollution over California: Ozone formation and air quality simulations, *Atmospheric*
808 *Environment*, 56: 45-51. doi:10.1016/j.atmosenv.2012.03.046, 2012.

809 Singh, H. B., L. Salas, D. Herlth, R. Kolyer, E. Czech, W. Viezee, Q. Li, D. J. Jacob, D. Blake, G. Sachse, C. N.
810 Harward, H. Fuelberg, C. M. Kiley, Y. Zhao, and Y. Kondo. In situ measurements of HCN and
811 CH₃CN over the Pacific Ocean: Sources, sinks, and budgets, *Journal of Geophysical Research-*
812 *Atmospheres*, 108. doi:10.1029/2002jd003006, 2003.

813 Sofiev, M., T. Ermakova, and R. Vankevich. Evaluation of the smoke-injection height from wild-land fires
814 using remote-sensing data, *Atmospheric Chemistry and Physics*, 12: 1995-2006.
815 doi:10.5194/acp-12-1995-2012, 2012.

816 Strand, T. M., N. Larkin, K. J. Craig, S. Raffuse, D. Sullivan, R. Solomon, M. Rorig, N. Wheeler, and D.
817 Pryden. Analyses of BlueSky Gateway PM_{2.5} predictions during the 2007 southern and 2008
818 northern California fires, *Journal of Geophysical Research-Atmospheres*, 117.
819 doi:10.1029/2012jd017627, 2012.

820 Urbanski, S., V. Kovalev, A. Petkov, A. Scalise, C. Wold, and W. M. Hao. Validation of smoke plume rise
821 models using ground-based lidar. in C. M. U. Neale and A. Maltese (eds.), *Remote Sensing for*
822 *Agriculture, Ecosystems, and Hydrology Xvi*. 2014.

823 Warneke, C., M. Trainer, J. A. de Gouw, D. D. Parrish, D. W. Fahey, A. R. Ravishankara, A. M.
824 Middlebrook, C. A. Brock, J. M. Roberts, S. S. Brown, J. A. Neuman, B. M. Lerner, D. Lack, D. Law,
825 G. Hubler, I. Pollack, S. Sjostedt, T. B. Ryerson, J. B. Gilman, J. Liao, J. Holloway, J. Peischl, J. B.
826 Nowak, K. C. Aikin, K. E. Min, R. A. Washenfelder, M. G. Graus, M. Richardson, M. Z. Markovic, N.
827 L. Wagner, A. Welti, P. R. Veres, P. Edwards, J. P. Schwarz, T. Gordon, W. P. Dube, S. A. McKeen,
828 J. Brioude, R. Ahmadov, A. Bougiatioti, J. J. Lin, A. Nenes, G. M. Wolfe, T. F. Hanisco, B. H. Lee, F.
829 D. Lopez-Hilfiker, J. A. Thornton, F. N. Keutsch, J. Kaiser, J. Q. Mao, and C. D. Hatch.
830 Instrumentation and measurement strategy for the NOAA SENEX aircraft campaign as part of
831 the Southeast Atmosphere Study 2013, *Atmospheric Measurement Techniques*, 9: 3063-93.
832 doi:10.5194/amt-9-3063-2016, 2016.

833 Wiedinmyer, C., S. K. Akagi, R. J. Yokelson, L. K. Emmons, J. A. Al-Saadi, J. J. Orlando, and A. J. Soja. The
834 Fire INventory from NCAR (FINN): a high resolution global model to estimate the emissions from
835 open burning, *Geoscientific Model Development*, 4: 625-41. doi:10.5194/gmd-4-625-2011, 2011.

836 Wiedinmyer, C., B. Quayle, C. Geron, A. Belote, D. McKenzie, X. Y. Zhang, S. O'Neill, and K. K. Wynne.
837 Estimating emissions from fires in North America for air quality modeling, *Atmospheric*
838 *Environment*, 40: 3419-32. doi:10.1016/j.atmosenv.2006.02.010, 2006.

839 Wotawa, G., and M. Trainer. The influence of Canadian forest fires on pollutant concentrations in the
840 United States, *Science*, 288: 324-28. doi:10.1126/science.288.5464.324, 2000.

841 Xu, L., A. M. Middlebrook, J. Liao, J. A. de Gouw, H. Y. Guo, R. J. Weber, A. Nenes, F. D. Lopez-Hilfiker, B.
842 H. Lee, J. A. Thornton, C. A. Brock, J. A. Neuman, J. B. Nowak, I. B. Pollack, A. Welti, M. Graus, C.
843 Warneke, and N. L. Ng. Enhanced formation of isoprene-derived organic aerosol in sulfur-rich
844 power plant plumes during Southeast Nexus, *Journal of Geophysical Research-Atmospheres*,
845 121: 11137-53. doi:10.1002/2016jd025156, 2016.

846 Yarwood, G., S. Rao, M. Yocke, and G. Whitten. Updates to the Carbon Bond Chemical Mechanism:
847 CB05, *Technical Report RT-0400675 ENVIRON International Corporation Novato, CA, USA*. 2005.

848 Zhang, X. Y., S. Kondragunta, and B. Quayle. Estimation of Biomass Burned Areas Using Multiple-
849 Satellite-Observed Active Fires, *IEEE Transactions on Geoscience and Remote Sensing*, 49: 4469-
850 82. doi:10.1109/tgrs.2011.2149535, 2011.

851